UFMC-based Wideband Spectrum Sensing for Cognitive Radios in Non-Gaussian Noise

Djamel Eddine Kebiche

Department of Electrical & Computer Engineering

McGill University

Montreal, Canada

August 2017

A thesis submitted to McGill University in partial fulfillment of the requirements for the degree of Master.

2017/08/14

Abstract

Cognitive radio (CR) is an important technology that allows to deal with spectrum congestion, where secondary applications (users) attempt to access a frequency band that is reserved for a primary application. A challenging function for a CR is to sense a frequency band and detect the absence or presence of a licensed user, a task referred to as *spectrum sensing*. Moreover, another challenging task in CR networks is to perform spectrum sensing in environments characterized by non-Gaussian noise distributions. While existing literature focuses mainly on the Gaussian noise model assumption, the latter does not properly characterize all the various noise types found in practical CR systems.

In this thesis, we investigate the performance of the recently proposed Rao-test based detector under non-Gaussian noise for wideband spectrum sensing in a multi-carrier transmission framework. Specifically, we incorporate this detector into the universal filtered multicarrier (UFMC) modulation scheme envisaged for high data rate 5G wireless systems. Through numerical simulations, we show that the Rao-test based detector combined with UFMC outperforms the traditional OFDM based system in a realistic non-Gaussian noise environment.

Sommaire

La radio cognitive (CR) est une technologie importante qui permet de traiter la congestion du spectre, où les applications (utilisateurs) secondaires tentent d'accéder à une bande de fréquence réservée à une application primaire. Une tâche difficile pour une CR est de détecter l'absence ou la présence d'un utilisateur autorisé dans une bande de fréquence determinée, une tâche appelée détection de spectre. De plus, une autre tâche difficile dans les réseaux CR consiste à effectuer une détection de spectre dans des environnements caractérisés par des distributions de bruit non-Gaussien. Bien que la littérature existante se concentre principalement sur l'hypothèse du modèle de bruit Gaussien, ce dernier ne caractérise pas correctement tous les différents types de bruit qui surviennent en pratique.

Dans ce mémoire, nous étudions la performance du détecteur Rao dans des environnements de bruit pratique non-Gaussien pour la détection du spectre à large bande dans une structure à porteuses multiples. Plus précisément, nous incorporons ce détecteur dans le système Universal Filtered Mulitcarrier (UFMC). Grâce à des simulations, nous montrons que le détecteur à base de test Rao combiné avec UFMC surpasse le système OFDM traditionnel dans un environnement de bruit pratique non-Gaussien.

Contents

Acknowledgements

The completion of this research would not have been possible without the help and support of many people that I would like to acknowledge. Foremost, I want to thank my advisor, Benoit Champagne, for his insightful guidance, patience, and rigorous care for details throughout my graduate studies. Moreover, thanks to Prof. Champagne, I greatly deepened my knowledge in the fields of communications and signal processing and also developed the taste for research. I am also grateful to Prof. Champagne for his financial support through research contracts with InterDigital Canada Ltée. Special mention to Dr. Afshin Haghighat and other staff members at InterDigital Canada Ltée for their constructive suggestions during various progress meetings. I would also like to thank the Department of Electrical and Computer Engineering at McGill University for their administrative support.

Many thanks are due to my friends and colleagues at the Telecommunications and Signal Processing Laboratory with whom I have had the pleasure to be acquainted: Ali Baghaki, Ryan Razani, Hao Li, Jiaxin Yang, Hanwook Chung, Alireza Morsali, and Vidhyasagar Mani. I would like to specially thank Ali Baghaki for his great support and guidance throughout my research. I would also like to thank my friend, Cameron Berge, for his continued moral support and motivation.

Finally, I would like to express my thanks to my family members for their support through all my endeavours. In particular, I am very grateful to my father Mustapha, and my mother Ania, for their unconditional love, support, and encouragement, without which none of my life's accomplishments would have been possible.

List of Figures

Notation

$\|x\|$	Absolute value of scalar or complex number
$E[\cdot]$	Expected value of random variable
Var$[\cdot]$	variance of random variable
$*$	Linear convolution operator
$Q(\cdot)$	Tail probability of normal random variable
$Q_N(\cdot,\cdot)$	Generalized Marcum's Q function with order N
$\mathcal{CN}(\mu,\sigma^2)$	Complex circular Gaussian distribution with mean μ and variance σ^2
$I_N(\cdot)$	Bessel function of the first kind and order N
$\chi^2_N(\cdot)$	Chi-Squared distribution with N degrees of freedom
$\chi^2_N(\xi)$	Non-central Chi-Squared distribution with N degrees of freedom and non-central parameter ξ
$\Gamma(\cdot)$	Gamma function
$\Gamma(\cdot,\cdot)$	Upper incomplete Gamma function
$\mathbb{Z}$	Set of all integers, i.e. $\{\ldots,-2,-1,0,1,2,\ldots\}$

List of Acronyms

UFMC	Universal Filtered Multicarrier
OFDM	Orthogonal Frequency Division Multiplexing
CR	Cognitive Radio
SU	Secondary User
PU	Primary User
FSA	Fixed Spectrum Access
DSA	Dynamic Spectrum Access
FCC	Federal Communications Commission
SNR	Signal-to-Noise Ratio
MCM	Multicarrier Modulation
FBMC	Filterbank Multicarrier
FMT	Filtered Multitone
CMT	Cosine Multitone
OQAM	Offset Quadrature Amplitude Modulation
ICI	Intercarrier Interference
ISI	Intersymbol Interference
AWGN	Additive White Gaussian Noise
GGDN	General Gaussian Distributed Noise
PDF	Probability Density Function
ROC	Receiver Operating Characteristic
P_d	Probability of Detection
P_{fa}	Probability of False Alarm
GLRT	Generalized Likelihood Ratio Test
FIR	Finite Impulse Response

FFT	Fast Fourier Transform
DFT	Discrete Fourier Transform
IDFT	Inverse Discrete Fourier Transform
PSD	Power Spectral Density
RF	Radio Frequency
DC	Dolph-Chebyshev
CP	Cyclic Prefix
SER	Symbol Error Rate
TTI	Transmission Time Interval
WSS	Wide-Sense Stationary
WSC	Wide-Sense Cyclostationary
LLRT	Log-Likelihood Ratio Rest

Chapter 1

Introduction

In this chapter, we first give a concise overview on the problem of wideband spectrum sensing for CR systems in non-Gaussian noise environments. Then, a literature survey on more specific topics pertinent to the research conducted in this work, including prominent spectrum sensing techniques and multicarrier modulation (MCM) frameworks. This is followed by a summary of the main objective and technical contributions of the thesis. Finally, the organization of the thesis is outlined.

1.1 Spectrum Allocation and Cognitive Radios

The need for higher data rates and wider signal bandwidth emerges from the growing demand of wireless applications and the transition from voice-only to multimedia applications, such as video streaming, internet browsing, etc. [1]. Traditionally, a Fixed Spectrum Access (FSA) policy has been adopted to support various wireless applications on a non-interfering basis. FSA assigns a piece of spectrum to one or more licensed users and only those users have the right to access that spectrum [1]. Nowadays, the majority of spectral resources available for wireless communications below 6GHz have been licensed and new applications will not have access to the radio spectrum with a static frequency allocation. However, studies have shown that even though the regulated radio spectrum has been fully occupied, vast portions of the licensed spectra are rarely used [2, 3]. For example, actual measurements of the spectrum utilization taken in downtown Berkley (California, USA), measured in average power measurements at a given time of day, as seen in Fig. 1.1, show a spectrum utilization of around 0.5% in the frequency band of 3-4GHz and only 0.3% in

the 4-5GHz frequency band [3]. This reveals that we have in fact spectrum abundance and

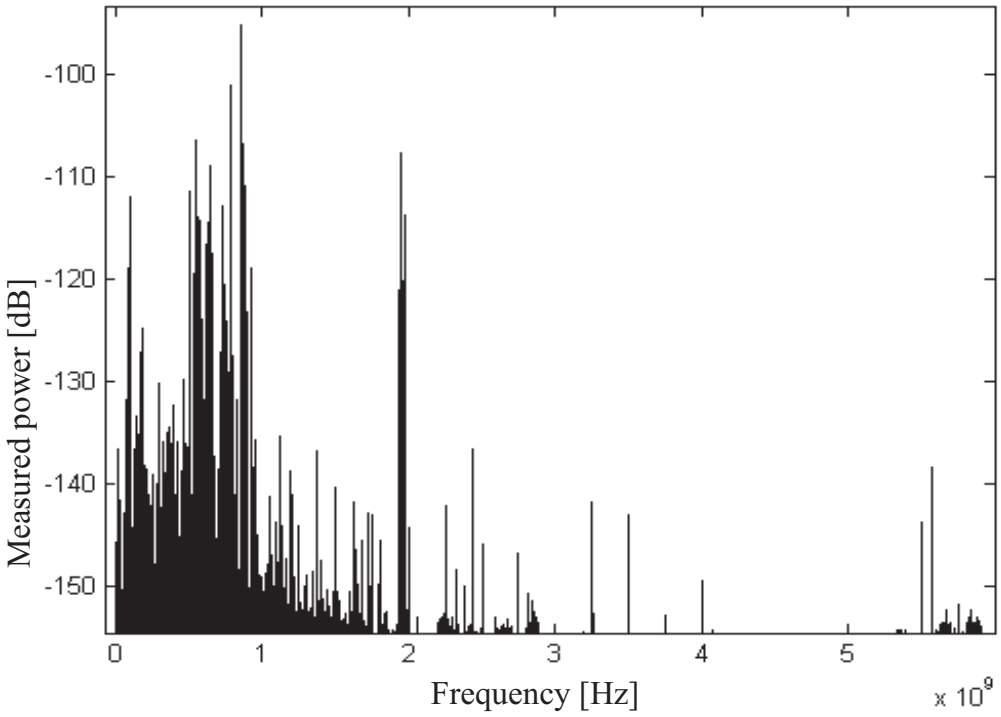

Fig. 1.1 Spectrum usage measurements in downtown Berkley [3]

that spectrum shortage is only an effect of the regulatory and licensing process. Therefore, new ways of exploiting the available spectrum are needed.

Cognitive radio (CR) has emerged as an innovative solution to the spectrum congestion problem by enabling opportunistic usage of the frequency bands that are not heavily used by licensed users [1]. According to the FCC CR can be defined as follows: "A radio or system that senses its operational electromagnetic environment and can dynamically and autonomously adjust its radio operating parameters to modify system operation, such as maximize throughput, mitigate interference, facilitate interoperability, access secondary markets." [2]. In the context of CR, primary users (PU) are defined as licensed users who have a higher priority on the usage of a specific part of the spectrum. Secondary users (SU) are defined as unlicensed CR users who can exploit the spectrum in a non-interfering manner to PUs. We refer to spectrum opportunity as chuncks of the available frequency band that are not being used simultaneously by the PU of that band.

Dynamic Spectrum Access (DSA) is an alternative spectrum allocation policy that can exploit spectrum opportunity, where SUs equipped with CRs can also access the allocated spectrum as long as the licensed band is unoccupied [1]. Withing the DSA framework, wireless networks equipped with CR capabilities must fulfill four main functions:

- **Spectrum sensing** is the task of determining spectrum availability and detect the presence of PUs. The detection problem is formulated as a binary hypothesis test where one compares a test statistic, dependent on the signal at the receiver-end, to a noise threshold.
- **Spectrum management** is to predict how long the spectrum holes are likely to remain available for SUs.
- **Spectrum sharing** has the objective to distribute unused spectrum among the unlicensed SUs.
- **Spectrum mobility** aims to perform seamless channel switchover, when a PU arrives in the licensed channel, while sustaining the performance of ongoing SU communications.

1.2 Spectrum Sensing in Non-Gaussian Noise

The focus of this thesis is on spectrum sensing since it is the first and most crucial component for the establishment of a CR link. Many modern spectrum sensing techniques have been developed, exploiting various properties of PUs and noise signals, in order to allow CRs to detect the presence of PU signal transmissions. A matched filter (MF) detection approach, where the received signal is demodulated by convolving it with a filter that is a mirror and time shifted version of the PU signal, is considered in [4–7]. This scheme achieves good detection under low signal-to-noise ratio (SNR) and is optimal when the primary signal is known. This approach however requires perfect knowledge of the PU's signal features such as bandwidth, operating frequency, modulation type, and so on which are most often not available in practice. Cyclostationary methods, where PU transmissions are detected by exploiting the cyclostationarity and periodicity features of PU signals, are considered in [8–14]. These methods enable to differentiate PU's signals from the wide sense stationary background noise by exploiting cyclostationary properties, i.e. specific

periodicity properties in the signal statistics such as the mean and autocorrelation function. However, the computational cost of such an approach is relatively high due to the requirement of calculating a two dimensional autocorrelation function depending on cyclic frequency and time lag. In spite of these developments, spectrum sensing based on energy detection remains the most recurrent technique because of its low computational and implementation complexity [15–20]. Furthermore, it is considered as a convenient blind detection approach since the receiver does not need *a priori* knowledge on the primary user's signal. The basic idea behind energy detection is that the PU signal is detected by comparing its energy measured at the receiver end with a threshold depending on the noise floor.

Over the years, many investigations have been conducted on the characteristics of noise in urban environments, such as man-made radio frequency (RF) noise and low frequency atmospheric noise [21]. Results have shown that these impairments tend to exhibit probability density functions (PDF) with tails decaying at lower rates than the traditional Gaussian PDF tails. This implies that they are more likely to produce observations with larger magnitudes than the Gaussian model would predict [21]. The energy detector is optimized with respect to a Gaussian noise environment. Consequently, when non-Gaussian noise impairments are present, the detector's performance is reduced considerably. A Rao-test based detector, which employs non-linear characteristics to reduce the influence of large-magnitude observations on the test statistic, has been recently proposed in [22] to overcome such limitations. In particular, the use of this detector in non-Gaussian noise shows to significantly enhance the detection performance, as compared to the energy detector.

1.3 Wideband Spectrum Sensing and Multicarrier Communications for Cognitive Radios

All the sensing techniques mentioned above are referred to as narrowband sensing techniques, since they focus on exploiting spectral opportunities over a narrow frequency range. However, CR networks will eventually be required to exploit spectral opportunities over a wider frequency range exceeding several hundreds of MHz in order to achieve considerable opportunistic throughput. Wideband spectrum sensing aims to sense a frequency band that exceeds the coherence bandwidth of the wireless channel [23]. In this case,

narrowband sensing techniques cannot be employed directly as they make a binary decision on the whole spectrum, thereby preventing the identification of individual spectral opportunities that manifest within the wider spectrum. A simple approach is to divide the wideband spectrum into a series of contiguous narrower subbands, through the application of Fourier transform or filter bank techniques on the received signal. Subsequently, narrowband sensing is applied in each subband to identify individual spectral opportunities. A more sophisticated approach consists in combining test statistics from multiple subbands and performing an (optimal) joint detection of the PU signals over the larger frequency spectrum, as presented in [24, 25]. Within this context, the use of a proper filtering scheme for separating the PU and SU signals in the frequency domain is of paramount importance.

MCM techniques are the main option for data transmission in the physical layer of modern telecommunication systems, such as 4G networks; they are preferred over single carrier modulation due to several benefits [26]. These techniques are also suitable for dividing the wideband spectrum into a series of contiguous narrower subbands for spectral estimation. The main advantage of employing MCM for CR systems is that these techniques may be used for both transmission and spectral estimation or sensing. A multicarrier transceiver, in a setting where SUs equipped with CR capabilities aim to dynamically fill spectrum holes, must exhibit two major properties [27]. Firstly, the CR transmitter must be able to confine the spectral content of the transmitted signal within the spectrum holes. In other words, the attenuation applied to signals outside of the band should be maximized. Secondly, the receiver should also be able to avoid the interference from other external signals transmitted outside the chosen band.

Among the MCM techniques, orthogonal frequency division multiplexing (OFDM) has been largely adopted in many 4G and pre-4G cellular networks, like mobile WiMAX and LTE due to its simplicity of implementation. It has also received considerable attention for CRs since the fast Fourier transform (FFT) can be used to demodulate an OFDM signal and also for spectral analysis [26]. However, OFDM suffers from high sidelobe levels resulting from the use of rectangular filtering shape in the time domain. This filtering is characterized by a sinc magnitude response in frequency and does not therefore satisfy the first requirement. Moreover, for spectrum sensing applications, these large sidelobes will result in spectral leakage, leading to spectral estimates in bands with low energy levels to be biased [28]. That is, the CR will have difficulty distinguishing bands with PU signals having low energy from bands containing only noise. This will cause unwanted interference

to the PU when the SU does not detect the PU signal and transmits over the band.

Filterbank multicarrier (FBMC) methods, where the rectangular window is replaced by filters that decay smoothly and are characterized with a magnitude response having lower sidelobes, have been studied by many researchers for upcoming 5G applications to address the shortcomings of OFDM [28]. Filtered multitone (FMT) presented in [29], where the filters are exponentially modulated and the subcarriers spectra do not overlap, has guards bands added to achieve orthogonality between subcarriers. The authors in [30] present a cosine modulated multitone scheme (CMT) where the filters are cosine modulated instead. The analysis of an OFDM/OQAM system where the in-phase and quadrature QAM components are separated in time by half a symbol period (OQAM) is presented in [31]. Nonetheless, these filterbank techniques can be very complex and filters lengths can be very large. An alternative and promising scheme, universal filtered multicarrier (UFMC) combines the simplicity of OFDM with the advantages of FBMC to minimize spectral leakage or maximize out-of-band rejection for future CR applications [32–38]. That is, UFMC significantly reduces the effect of sidelobe interference compared to OFDM while using shorter filter lengths reducing the cost of implementation compared to FBMC.

1.4 Thesis Objective and Contribution

Most of the current literature on wideband spectrum sensing for CR focuses on OFDM based techniques to break the wideband spectrum into several narrower subbands. This is followed by energy detection, once per subband, also known as the periodogram spectral estimator. Some of the current literature also considers the use of FBMC replacing the rectangular window by a window function leading to better spectral properties. Even though the latter offers a better out-band-rejection compared to OFDM, it suffers from a few drawbacks such as long filters and high complexity of implementation. As a result, most recently, UFMC where filtering is applied over a group of consecutive subcarriers has been proposed to alleviate the complexity issues of FBMC while benefiting from its spectral advantages [32].

Moreover, most of the current literature on blind wideband spectrum sensing considers the Gaussian noise model assumption and consequently adopt the traditional energy detector. Nevertheless, as mentioned previously, the simple Gaussian noise model may not be appropriate to characterize impairments such as urban and man-made RF noise encoun-

tered in practical environments. For this reason, the use of non-linear detectors has been gaining much attention recently [22].

The objective of this thesis is to investigate the advantages of the Rao test based non-linear detector presented in [22] over the traditional energy detector for wideband spectrum sensing subject to non-Gaussian noise impairments in a multicarrier framework. Specifically, we incorporate the Rao detector into the UFMC modulation scheme in [32] which aims to combine the benefits of FBMC and the simplicity of OFDM. We demonstrate that the Rao-test based detector combined with UFMC outperforms the traditional OFDM system in a realistic non-Gaussian noise environment through numerical simulations. Overall, our results show that the Rao detector incorporated in UFMC offers a suitable scheme for wideband spectrum sensing in CR applications for future 5G networks.

1.5 Thesis Organization

The rest of this thesis is organized as follows. In chapter II, we briefly cover wideband spectrum sensing techniques from the recent literature. We present in more detail the Rao-test based detector optimized for non-Gaussian noise. In chapter III, we begin by giving a brief overview of MCM and then describe the UFMC system operation along with the prototype filter design. In chapter IV, we explain how to incorporate the Rao detector into the UFMC scheme. In chapter V, the detection performance of the Rao detector integrated into the UFMC scheme for wideband spectrum sensing in non-Gaussian noise is evaluated via simulations and compared to other benchmark approaches. Finally, the thesis is summarized and conclusions are drawn in chapter VI.

Chapter 2

General Wideband Spectrum Sensing Techniques

In this Chapter, spectrum sensing techniques for a wideband channel are reviewed. The chapter begins with a formulation of the wideband CR spectrum sensing problem and the fundamentals of PU signal detection. Then, detection algorithms based on PU cyclostationary features and MF are briefly outlined. Finally, techniques optimized for Gaussian and non-Gaussian noise with no a priori knowledge of PU signal characteristics, such as the energy and Rao detector, are discussed in detail. The latest will serve as a basis for the development of UFMC-based wideband spectrum sensing in non-Gaussian noise environments, as presented in Chapter 4

2.1 Multiband PU Spectrum Sensing System

As discussed in Section 1.1, CR will be required to detect spectral opportunities over a wider frequency range while narrowband sensing techniques may not be applied directly. For this reason, we consider a general wideband system where the wideband spectrum is divided into B non-overlapping narrow subbands and subsequently, narrowband spectrum techniques are applied in each subband. Some of these subbands might not be used by PUs and are therefore available for opportunistic SU access. Fig. 2.1 illustrates the spectrum availability for a given multicarrier wideband communication channel. As we can see, at a given time, some of these subbands (depicted as white rectangles) can be used opportunistically by SUs. The decision of a particular SU on the presence or absence of a PU for subband

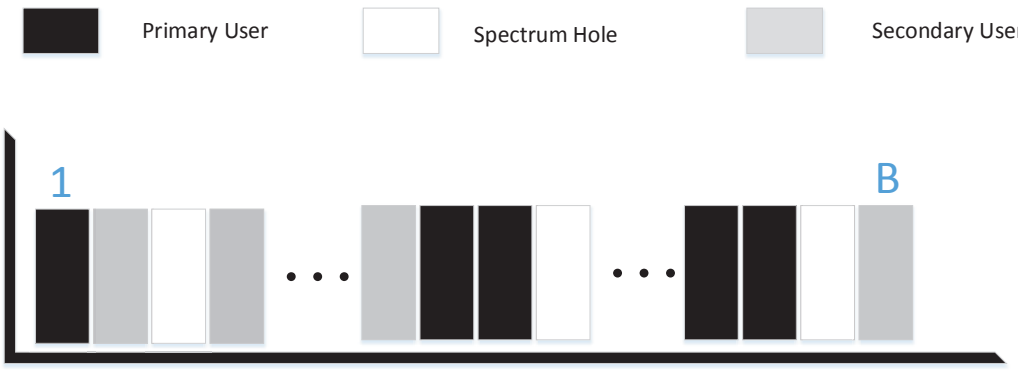

Fig. 2.1 Illustration of opportunistic spectrum access

$j \in \{1, ..., B\}$ can be formulated as a binary hypothesis testing problem as follows [24]:

$$H_{0,j} : R_j(n) = W_j(n) \tag{2.1}$$

$$H_{1,j} : R_j(n) = H_j S_j(n) + W_j(n) \tag{2.2}$$

where $n = 0, ..., N-1$ is the discrete-time index, N is the total number of samples in the observation window, $R_j(n)$ is the received signal sample at time n, $S_j(n)$ is the PU signal component, $W_j(n)$ is the complex additive white Gaussian noise (AWGN) with zero mean and variance σ_w^2, and H_j is the flat fading channel gain between the PU and SU for subband j. The SU has to decide between two hypotheses, that is: $H_{0,j}$ representing the presence of only noise in the j^{th} subband, implying that it is vacant and thus available for opportunistic access; and $H_{1,j}$ representing the presence of a PU signal with noise, implying that the j^{th} subband is occupied. The decision task is accomplished by forming a test statistic $T\{R_j(n)\}$ from the received signal $R_j(n)$ and comparing that statistic with a predetermined threshold λ_j. This operation can be formulated as follows:

$$T\{R_j(n)\} \underset{H_{0,j}}{\overset{H_{1,j}}{\gtrless}} \lambda_j \tag{2.3}$$

The performance of the detection algorithm can be assessed in terms of its receiver operating characteristic (ROC) curve. This curve plots the probability of detection (P_d) versus the probability of false alarm (P_{fa}) as obtained by varying the detection threshold. P_{fa} is the

probability that the test incorrectly decides that the considered frequency is occupied when it is actually not. P_d is the probability of detecting a signal on the considered frequency band when it truly is present. The operating point of a detector is chosen along its ROC curve by adjusting the threshold λ_j. To achieve good detection performance in a given setting, we therefore need to select an adequate test statistic for the system model under consideration and correctly set the decision threshold.

2.2 Cyclostationarity Feature Detection

The information signal transmitted by a PU in practical communication systems always contain specific features that can be exploited for detection. For instance, due to the inherent periodicities such as modulation rate and carrier frequency, the statistics of the transmitted PU signal in most cases are periodic. These features, most commonly referred to as cyclostationary features, enable the SU to distinguish cyclostationary PU signals from the wide-sense stationary (WSS) background noise signals [39].

Indeed, a PU signal is typically a modulated sinusoidal carrier and therefore can be modeled as a wide-sense cyclostationary (WSC) stochastic process. This means that its second order statistics, such as the mean and autocorrelation functions, are both periodic with period T. That is, for the discrete time PU signal component $S_j(n)$, we have the following relations [39]:

$$E[S_j(n)] = E[S_j(n+T)] \tag{2.4}$$

$$\begin{aligned} R_{\text{ss}}(n,\tau) &\triangleq E[S_j(n)S_j^*(n+\tau)] \\ &= R_{\text{ss}}(n+T,\tau) \end{aligned} \tag{2.5}$$

where $R_{\text{ss}}(n,\tau)$ is the autocorrelation function of $S_j(n)$ and τ is a discrete time lag. For modulated PU signals, T is a function of the symbol period and the carrier frequency of the processed signal. Moreover, the autocorrelation function $R_{\text{ss}}(n,\tau)$ of the WSC process $S_j(n)$ can also be represented by its Fourier series expansion expressed as follows:

$$R_{\text{ss}}(n,\tau) = \sum_{l\in\mathbb{Z}} R'_{\text{ss}}(\alpha,\tau)e^{2\pi\jmath\alpha n} \tag{2.6}$$

where $\alpha \equiv l/T$, for $l \in \mathbb{Z}$, is the cyclic frequency represented as an integer multiple of the

reciprocal of T. The Fourier coefficients $R'_{\text{ss}}(\alpha, \tau)$, also known as the cyclic autocorrelation at cyclic frequency α, are given by:

$$R'_{\text{ss}}(\alpha, \tau) = \frac{1}{N} \sum_{n=0}^{N-1} R_{\text{ss}}(n, \tau) e^{-2\pi \jmath \alpha n} \tag{2.7}$$

We can construct a spectrum sensing detector that exploits cyclostationarity, if we know some of the cyclic characteristics of the PU signal, such as the symbol length and carrier frequencies. One method is to exploit cyclostationarity based on an estimate of the cyclic autocorrelation of the receiver signal $R_j(n)$ corresponding to subband j obtained at a specific cyclic frequency. The cyclic autocorrelation is estimated by [39]:

$$\hat{R}_{\text{rr}}(\alpha, \tau) = \frac{1}{N} \sum_{n=0}^{N-1} R_j(n) R_j^*(n + \tau) e^{-2\pi \jmath \alpha n} \tag{2.8}$$

The detector's test statistic, which depends on the statistical properties of the PU signal component, is derived from the following log-likelihood ratio test (LLRT) [12]:

$$T\{R_j(n)\} = \ln\Big(\frac{f(\hat{R}_{\text{rr}}(\alpha, \tau)|H_{0,j})}{f(\hat{R}_{\text{rr}}(\alpha, \tau)|H_{1,j})}\Big) \tag{2.9}$$

where $f(\hat{R}_{\text{rr}}(\alpha, \tau)|H_{0,j})$ and $f(\hat{R}_{\text{rr}}(\alpha, \tau)|H_{1,j})$ denote the conditional PDFs of $\hat{R}_{\text{rr}}(\alpha, \tau)$ under $H_{0,j}$ and $H_{1,j}$ respectively. The decision rule is implemented as [12]:

$$T\{R_j(n)\} \underset{H_{0,j}}{\overset{H_{1,j}}{\gtrless}} \ln(\lambda_j) \tag{2.10}$$

where $\ln(\lambda_j)$ is the threshold. Only one or a few cyclic frequencies are used for detection in practice and this is most often sufficient to achieve good detection performance [39]. In particular, the cyclostationarity detector of [11] extends the above detector to multiple cyclic frequencies achieving better detection. It is important to notice that the detection scheme based on cyclic autocorrelation requires *a priori* knowledge of the cyclic frequency α which is a function of PU signal's symbol rate and carrier frequency. In practice, however, the cyclic frequencies are not generally available.

2.3 Matched Filter Detection

MF detection, also known as the coherent detection, is the optimal spectrum sensing scheme when perfect knowledge of the PU signal $S_j(n)$ is available *a priori*. Indeed, this approach can match and correlate the already known PU signal with the received signal, thereby achieving maximum SNR in presence of additive noise [6].

To show that MF detection achieves maximum SNR, we consider the filtering and sampling at time $n = N - 1$ of $R_j(n)$ as expressed by:

$$r_j = \sum_{\tau=0}^{N-1} R_j(\tau) G(n - \tau) \tag{2.11}$$

where r_j is the output of the filtering and sampling operation and $G_j(n)$ is the linear, causal time-invariant filter. Because $R_j(n) = S_j(n) + W_j(n)$, it follows that:

$$r_j = s_j + w_j \tag{2.12}$$

where s_j and w_j are the signal and noise components at the output of the filter. We define the SNR at time $n = N - 1$ as:

$$\text{SNR} = \frac{|s_j|^2}{E[|w_j|^2]} \tag{2.13}$$

By invoking the Cauchy-Schwarz inequality [40], it can be shown [7] that the maximum value of SNR in obtained when the filter $G_j(n) = S_j^*(N - 1 - n)$, which corresponds to the so-called MF solution. By substituting $G_j(n) = S_j^*(N - 1 - n)$ into (2.11), we can write:

$$r_j = \sum_{\tau=0}^{N-1} R_j(\tau) G_j(N - 1 - \tau) \tag{2.14}$$

$$= \sum_{\tau=0}^{N-1} R_j(\tau) S_j^*(\tau) \tag{2.15}$$

Therefore, given N observations from the signal $R_j(n)$, the test statistic for the MF ap-

proach can be formulated as follows [6]:

$$T_{E,j} \triangleq T\{R_j(n)\} = \sum_{n=0}^{N-1} R_j(n) S_j^*(n) \tag{2.16}$$

The decision rule is chosen as:

$$T\{R_j(n)\} \underset{H_{0,j}}{\overset{H_{1,j}}{\gtrless}} \lambda_j \tag{2.17}$$

where λ_j is the threshold.

Not only does this method requires complete knowledge of the PU signal, which is usually not available in practice, it suffers from a high implementation complexity as it requires multiple receive filters for all types of signal variations.

2.4 Non-Coherent Detection

2.4.1 Optimal Detector in Gaussian Noise Environment: Energy Detector

We first consider the spectrum sensing model within a Gaussian noise environment. The non-coherent energy detector, optimized for Gaussian noise environments (in the Neyman-Pearson sense), is one of the simplest approaches for deciding between hypotheses $H_{0,j}$ and $H_{1,j}$. It was first discussed by Urkowitz [15] as a binary hypothesis testing problem for the detection of deterministic signals in Gaussian noise environments and then investigated by Digham *et al.* in [16] for unknown signals. This detector is derived based on N observations of $R_j(n)$ and assuming a PU signal with unknown structure. The test statistic can be expressed as [6]:

$$T_E\{R_j(n)\} = \sum_{n=0}^{N-1} |R_j(n)|^2 \tag{2.18}$$

and the decision rule is chosen as:

$$T_E\{R_j(n)\} \underset{H_{0,j}}{\overset{H_{1,j}}{\gtrless}} \lambda_j \tag{2.19}$$

where λ_j is the corresponding test threshold.

To analyze the performance of the energy detector, we assume that the number of samples N is sufficiently large such that the PDF of the test statistic will approach a Gaussian distribution according to the central limit theorem. Therefore, we can model the test statistic $T_E\{R_j(n)\}$ under $H_{0,j}$ and $H_{1,j}$ as [17]:

$$H_{0,j} : T_{E,j} \sim \mathcal{CN}(E(T_{E,j}|H_{0,j}), Var(T_{E,j}|H_{0,j})) \tag{2.20}$$

$$H_{1,j} : T_{E,j} \sim \mathcal{CN}(E(T_{E,j}|H_{1,j}), Var(T_{E,j}|H_{1,j})) \tag{2.21}$$

In order to obtain analytic expressions for the probabilities of detection and false alarm of the energy detector, we need to derive expressions for the conditional mean and variance of the test statistic introduced in (2.18). The derivation of these expressions, which is presented in detail in appendix A, make use of the following formulas for the q^{th} order absolute moment of the complex Gaussian noise for subband j [41]:

$$E[|W_j(n)|^q] = \begin{cases} (2)^{q/2}\frac{\Gamma((q+1)/2)}{\sqrt{\pi}}\sigma_w^q, & q = 2, 4, 6, ... \\ 0, & q = 1, 3, 5, ... \end{cases} \tag{2.22}$$

Under $H_{0,j}$ and $H_{1,j}$, assuming complex Gaussian additive noise with zero mean and PU signal with unitary energy, the expectations and variances of the test statistic can be expressed with the help of (2.22) as:

$$E[T_{E,j}] = \begin{cases} N\sigma_w^2, & H_{0,j} \\ N(|H_j|^2 + \sigma_w^2), & H_{1,j} \end{cases} \tag{2.23}$$

$$Var[T_E\{R_j(n)\}] = \begin{cases} 2N\sigma_w^4, & H_{0,j} \\ N\Big(2\sigma_w^4 + 2|H_j|^2\sigma_w^2 - |H_j|^4\Big), & H_{1,j} \end{cases} \tag{2.24}$$

Under the Gaussian assumption for $T_{E,j}$, it follows that the probabilities of detection and

false alarm associated with the energy detector can be respectively written as [17]

$$P_{\mathrm{fa},j} = Pr(T_{E,j} > \lambda_j | H_{0,j}) = Q\Big(\frac{\lambda_j - E(T_{E,j}|H_{0,j})}{\sqrt{Var(T_{E,j}|H_{0,j})}}\Big) \tag{2.25}$$

$$P_{\mathrm{d},j} = Pr(T_{E,j} > \lambda_j | H_{1,j}) = Q\Big(\frac{\lambda_j - E(T_{E,j}|H_{1,j})}{\sqrt{Var(T_{E,j}|H_{1,j})}}\Big) \tag{2.26}$$

where $Q(x)$ is the tail probability of the normal random variable, define as:

$$Q(x) = \frac{1}{\sqrt{2\pi}} \int_x^\infty \mathrm{e}^{-t^2/2} dt. \tag{2.27}$$

2.4.2 Optimal Detector in General Gaussian Distributed (GGD) Noise Environment: Rao Detector

If non-Gaussian noise impairments are present, as discussed in Section 1.2, the energy detector's performance is significantly reduced. Therefore, we must model the noise differently such as to account for noise types characterized by PDFs with tails decaying at lower rates than the Gaussian PDF. We also need to consider a new test statistic that can account for the different tails. We first start by describing the new noise model.

Here, we assume that non-Gaussian noise occurring in practice can be modeled by a complex generalized Gaussian distribution (GGD), thereby allowing to control the tail characteristics by means of an adjustable parameter. Specifically, the PDF of a GGD with mean μ and variance σ_w^2 is expressed as follows [22]:

$$f_{\mathrm{GGD}}(w;\beta) = \frac{\beta}{2A(\beta,\sigma_w^2)\Gamma(1/\beta)} e^{-\left(\frac{|w-\mu|}{A(\beta,\sigma_w^2)}\right)^\beta} \tag{2.28}$$

where

$$A(\beta,\sigma_w^2) = \sqrt{\Big(\sigma_w^2 \frac{\Gamma(1/\beta)}{\Gamma(3/\beta)}\Big)} \tag{2.29}$$

$\Gamma(\nu)$ is the standard gamma function, i.e.,

$$\Gamma(\nu) = \int_0^\infty x^{\nu-1} \mathrm{e}^{-x} dx \tag{2.30}$$

and $\beta > 0$ is a shaping factor that controls the exponential decay rate of the PDF tail,

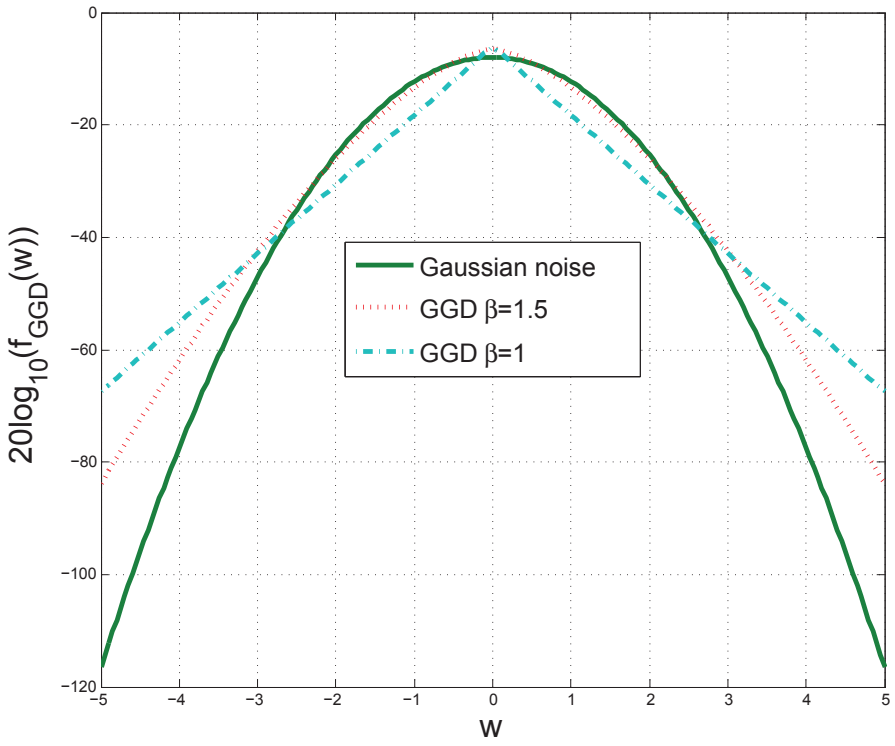

Fig. 2.2 PDF of GGD random variable for different β values and $\sigma_w^2 = 1$

allowing to model different noise behaviors. The PDF of the GGD is plotted in Fig. 2.2 showing the tail characteristics for different β values. The GGD reduces to the Gaussian distribution when $\beta = 2$ and to the Laplacian distribution when $\beta = 1$. Several types of noise sources found in practice tend to produce samples with higher magnitudes than what the Gaussian noise model would predict, i.e. corresponding to the case $\beta < 2$.

We first discuss the performance of the energy detector in the presence of GGD noise. To this end, we first develop expressions for the conditional mean and variance of the test statistic $T_{E,j}$ under the GGD noise model;then from the mean and variance, we derive the expressions of P_d and P_{fa}. We again assume that the number of samples N is large enough such that the PDF of $T_E\{R_j(n)\}$ will approach a Gaussian distribution even if the noise is GGD. The q^{th} order absolute moment of GGD noise in subband j, that is used to derive

the mean and variance of $T_{E,j}$ under non-Gaussian noise, is given by [22]:

$$E[|W_j(n)|^q] = \begin{cases} \left[\frac{\Gamma(1/\beta)}{\Gamma(3/\beta)}\right]^{q/2} \frac{\Gamma((q+1)/\beta)}{\Gamma(1/\beta)} \sigma_w^q & q = 2, 4, 6, ... \\ 0 & q = 1, 3, 5, ... \end{cases} \tag{2.31}$$

Using (2.31), the conditional mean and variance of $T_{E,j}$ under $H_{j,0}$ and $H_{j,1}$ can be obtained by following the steps in appendix B as:

$$E[T_{E,j}] = \begin{cases} N\sigma_w^2, & H_{0,j} \\ N(|H_j|^2 + \sigma_w^2), & H_{1,j} \end{cases} \tag{2.32}$$

$$Var[T_{E,j}] = \begin{cases} N\sigma_w^4 \Big(\frac{\Gamma(1/\beta)}{\Gamma(3/\beta)^2} \Gamma(5/\beta) - 1 \Big), & H_{0,j} \\ N\Big[\Big(\frac{\Gamma(1/\beta)}{\Gamma(3/\beta)^2} \Gamma(5/\beta) - 1 \Big) \sigma_w^4 + 2|H_j|^2 \sigma_w^2 - |H_j|^4 \Big], & H_{1,j} \end{cases} \tag{2.33}$$

The probabilities of detection and false alarm for the energy detector under GGD noise can then be obtained by substituting (2.32) and (2.33) into (2.25) and (2.26) respectively. Moreover, the probabilities of detection and false alarm are given in (2.25) and (2.26) respectively. Moreover, when $P_{fa,j}$ is given, the decision threshold λ_j of the energy detector can be expressed as [22]:

$$\lambda_j = \sigma_w^2 \left(\sqrt{N \Big(\frac{\Gamma(1/\beta)}{\Gamma(3/\beta)^2} \Gamma(5/\beta) - 1 \Big)} Q^{-1}(P_{fa,j}) + N \right) \tag{2.34}$$

and finally, by substituting (2.34) into (2.26), the $P_{d,j}$ can also written as:

$$\begin{aligned} P_{d,j} &= Q\Big(\frac{\sigma_w^2 \left(\sqrt{N \Big(\frac{\Gamma(1/\beta)}{\Gamma(3/\beta)^2} \Gamma(5/\beta) - 1 \Big)} Q^{-1}(P_{fa,j}) + N \right) - N(|H_j|^2 + \sigma_w^2)}{\sqrt{N \Big[\Big(\frac{\Gamma(1/\beta)}{\Gamma(3/\beta)^2} \Gamma(5/\beta) - 1 \Big) \sigma_w^4 + 2|H_j|^2 \sigma_w^2 - |H_j|^4 \Big]}} \Big) \\ &= Q\Big(\frac{\sqrt{\Big(\frac{\Gamma(1/\beta)}{\Gamma(3/\beta)^2} \Gamma(5/\beta) - 1 \Big)} Q^{-1}(P_{fa,j}) - \sqrt{N} \frac{|H_j|^2}{\sigma_w^2}}{\sqrt{\Big(\frac{\Gamma(1/\beta)}{\Gamma(3/\beta)^2} \Gamma(5/\beta) - 1 \Big) + 2\frac{|H_j|^2}{\sigma_w^2} - \frac{|H_j|^4}{\sigma_w^4}}} \Big) \end{aligned} \tag{2.35}$$

As discussed in Section 1.2, the energy detector's performance is greatly reduced when non-Gaussian noise impairments are present. This is because non-Gaussian noise is more likely to produce large-magnitude observations than would be predicted by a Gaussian model [21]. Therefore, we should expect the optimum detector in presence of non-Gaussian noise characterized by the GGD to employ some nonlinear characteristics, aiming to reduce the influence of large-magnitude observations on the test statistic [21].

The non-linear detector in [22], based on the Rao test, is optimized for GGD noise environments. As such, it can reduce the influence of high magnitude samples on the test statistic making it more reliable to indicate the presence or absence of a signal. Specifically, the Rao test statistic can be formulated as:

$$T_{R,j} \triangleq T_R\{R_j(n)\} = \phi(\beta) \sum_{n=0}^{N-1} (|R_j^{\mathrm{Re}}(n)|^{2(\beta-1)} + |R_j^{\mathrm{Im}}(n)|^{2(\beta-1)}) \tag{2.36}$$

where $R_j^{\mathrm{Re}}(n)$ and $R_j^{\mathrm{Im}}(n)$ represent the real and imaginary parts of the receiver signal respectively, i.e., $R_j(n) = R_j^{\mathrm{Re}}(n) + \jmath R_j^{\mathrm{Im}}(n)$, and $\phi(\beta)$ is defined as:

$$\phi(\beta) = \frac{\beta\Gamma(\frac{3}{\beta})^{\beta-1}}{(\beta-1)(\frac{\sigma_w^2}{2})^{\beta-1}\Gamma(\frac{1}{\beta})^{\beta-2}\beta\Gamma(1-\frac{1}{\beta})} \tag{2.37}$$

Similar to (2.20), the decision rule is given by:

$$T_R\{R_j(n)\} \underset{H_{0,j}}{\overset{H_{1,j}}{\gtrless}} \lambda_j \tag{2.38}$$

where λ_j is the decision threshold of the Rao detector for subband j. As we can see, similar to the energy detector, the test statistic $T_R\{R_j(n)\}$ is only a function of the shaping factor β, thereby requiring no *a priori* knowledge of the PU's signal, channel gains, or noise variance.

Next, we present formulas for the probabilities of detection and false alarm of the Rao test detector. As the number of samples N becomes large, the PDF of the Rao test statisitic approaches that of the generalized likelihood-ratio test (GLRT) statistic. Therefore, we

have [22]

$$H_{0,j} : T_{R,j} \sim \chi^2_{2N} \tag{2.39}$$

$$H_{1,j} : T_{R,j} \sim \chi^2_{2N}(\xi_j) \tag{2.40}$$

where χ^2_{2N} denotes a chi-squared PDF with $2N$ degrees of freedom while $\chi^2_{2N}(\xi_j)$ denotes a non-central chi-squared PDF with $2N$ degrees of freedom and non-centrality parameter ξ_j. The parameter ξ_j can be approximated as:

$$\xi_j = N \frac{2\beta(\beta-1)\Gamma(1-1\beta)\Gamma(3/\beta)}{\Gamma(1/\beta)^2} \frac{|H_j|^2}{\sigma_w^2} \tag{2.41}$$

Using the non-centrality parameter in (2.41) and the Rao detector's PDFs in (2.42) and (2.43) , we can also express the conditional PDF of $T_{R,j}$ as [22]:

$$H_{0,j} : p(t|H_{0,j}) = \frac{1}{2^N \Gamma(N)} t^{N-1} \mathrm{e}^{-t/2} \tag{2.42}$$

$$H_{1,j} : p(t|H_{1,j}) = \frac{1}{2}\Big(\frac{t}{\xi_j}\Big)^{N-1/2} \mathrm{e}^{-1/2(t+\xi_j)} I_{N-1}(\sqrt{(t\xi_j)}) \tag{2.43}$$

where

$$I_{N-1}(x) = \frac{\sum_{k=0}^{\infty} (x/2)^{2k+N-1}}{k!\Gamma(N-1+k+1)} \tag{2.44}$$

is the modified Bessel function of order $N-1$ and of the first kind for $x > 0$.
Finally, with the expressions in (2.42) and (2.43), the probabilities of detection and false alarm of the Rao-test based detector are given by

$$P_{\mathrm{fa},j} = Pr(T_{R,j} > \lambda_j | H_{0,j}) = \int_{\lambda_j}^{\infty} p(t|H_0, j)dt = \frac{\Gamma(N, \lambda_j/2)}{\Gamma(N)} \tag{2.45}$$

$$P_{\mathrm{d},j} = Pr(T_{R,j} > \lambda_j | H_{1,j}) = \int_{\lambda_j}^{\infty} p(t|H_1, j)dt = Q_N(\sqrt{\xi_j}, \sqrt{\lambda_j}) \tag{2.46}$$

where

$$\Gamma(u,v) = \int_v^\infty x^{u-1}\mathrm{e}^{-x}dx, \qquad u,v>0 \tag{2.47}$$

is the upper incomplete gamma function and

$$Q_N(u,v) = \frac{1}{u^{N-1}}\int_v^\infty x^N \mathrm{e}^{-(x^2+u^2)/2} I_{N-1}(ux)dx, \qquad u,v>0 \tag{2.48}$$

is the N^{th} order generalized Marcum Q function.

Chapter 3

Universal Filtered Multicarrier

As was discussed in Section 1.3, MCM can be used for both CR data transmission and dividing the wideband spectrum into narrow subbands for PU detection. We first start by giving an overview of MCM. Then, we briefly describe the traditional OFDM system operation for the sake of comparing with UFMC. Following this, we describe the UFMC system operation and present the associated prototype filter design. This will enable us to develop, in Chapter 4, the wideband spectrum sensing models of non-coherent UFMC-based detectors optimized for both Gaussian and GGD noise.

3.1 Overview of Multicarrier Modulation

The main idea behind MCM is to divide the transmitted stream of symbols into many different substreams and to send these in parallel over different orthogonal subchannels [42]. For a given system bandwidth, the number of subchannels is chosen such that their individual bandwidth is less than the channel coherence bandwidth, thereby ensuring a smaller intersymbol interference (ISI) on each subchannel. That is, consider a communication system with incoming data rate R and total bandwidth B, transmitting over a channel having a coherence bandwidth B_c. In this case, the transmitted signal will experience frequency selective fading if $B > B_c$. The basic premise of MCM is to divide the modulated system into K subchannels each having data rate $R_s = R/K$ and bandwidth $B_s = B/K$. Assuming that the number of channel K is large enough, the signal will now experience relatively flat fading as $B_s < B_c$. This means that the spectral characteristics of the transmitted signal will be preserved at the receiver with a variation only in the strength of the sig-

nal (i.e. amplitude and phase). Fig. 3.1 illustrates a multicarrier transmitter, where the

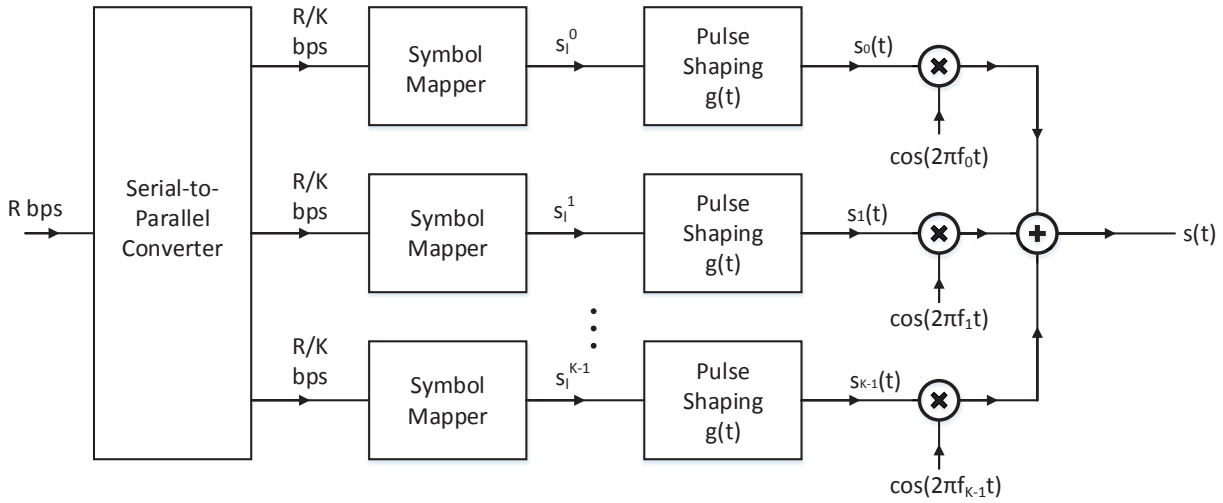

Fig. 3.1 Schematic representation of multicarrier transmitter

incoming bit stream is divided into K substreams via a serial-to-parallel converter. The first step is to convert each binary sequence into a corresponding sequence of symbols s_l^k via a symbol mapper, typically by means of quadrature amplitude modulation (QAM) or phase shift keying (PSK). Within each substream, each symbol is further multiplied by a pulse shaping waveform $g(t)$ which defines the signal's spectrum, resulting in a baseband waveform

$$s_k(t) = \sum_l s_l^k g(t - lT) \tag{3.1}$$

where $k = 0, 1, \ldots, K-1$ is the subcarrier index and T is the symbol duration. The waveforms $s_k(t)$ are up-converted to their proper frequency location in the passband, and then summed, to yield the following modulated output [42]:

$$s(t) = \sum_{k=0}^{N-1} s_k(t) \cos(2\pi f_k t). \tag{3.2}$$

The latter signal in then sent to the antenna circuit for radio transmission over the air. The modulation frequencies f_k are typically set to $f_k = f_0 + kB_s$.

During transmission, under the assumption $B_s < B_c$, the k^{th} subchannel will be affected

by flat fading with a corresponding gain $H(f_k)$, where $H(f)$ denotes the frequency response of the radio channel, as illustrated in Fig. 3.2. This is a fundamental property of MCM which makes channel equalization very easy to implement.

Fig. 3.3 illustrates the multicarrier receiver where the signal is first decomposed into subchannel components using a bank of filters. Channel equalization at the receiver is then realized by multiplying the k^{th} substream by $1/H(f_k)$, where the channel gains are assumed to be known. Subsequently, each substream is down-converted to passband and fed to a matched filter detector. Finally, the detected bits on each stream are combined via a parallel-to-serial converter, in order to reconstruct the transmitted binary sequence. In the next section, we present a popular digital implementation of MCM where there is no need for multiple modulator and demodulators.

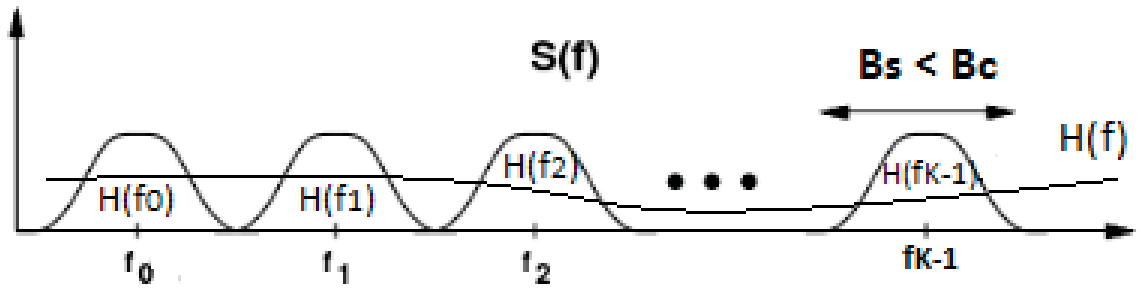

Fig. 3.2 Spectrum of transmitted MCM signal

3.2 OFDM

The requirement for separate modulators and demodulators on each subchannel was too complex for most systems implemented at the time MCM was conceived in the 1950's [42]. However, with the development of cheap and simple implementations of the discrete Fourier transform (DFT) and inverse discrete Fourier transform (IDFT), in the form of fast Fourier transform (FFT) algorithms, the multicarrier technique could be efficiently implemented digitally with these algorithms. Referred to as OFDM, this method is commonly employed nowadays in most of the standards for wireless transmissions [26]. In this section, we briefly

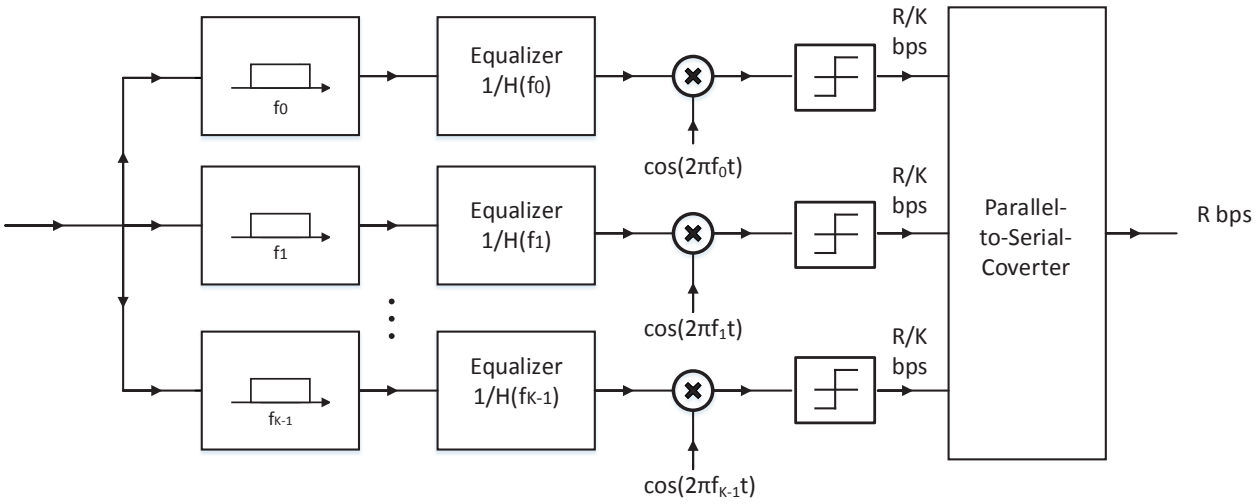

Fig. 3.3 Schematic representation of multicarrier receiver

describe the OFDM implementation of MCM, as it will serve as a comparison benchmark in our work.

3.2.1 OFDM Operation

The schematic representation of the OFDM implementation is shown in Fig. 3.4. The incoming data bit stream is passed through a serial-to-parallel converter where, at a given time instance, it is converted into a corresponding sequence of symbols denoted as X_k to be transmitted over each of the subcarriers with index $k = 0, 1, \ldots, K-1$. Each symbol belongs to a given constellation, e.g. M-QAM or PSK and in the case of adaptive modulation, different constellations can be used over different subcarriers [43]. The frequency components of the OFDM modulator are converted into discrete-time domain samples $x(l)$ by applying a K-point IDFT on the symbols X_k. This operation yields what we refer to as the OFDM symbol of length K which can be expressed as [42]:

$$x(l) = \frac{1}{K} \sum_{k=0}^{K-1} X_k \mathrm{e}^{2\pi \jmath lk/K} \tag{3.3}$$

where the index $l = 0, ..., K-1$. The sequence $x(l)$, which is obtained by linearly modulating the various subcarriers, provides the time-domain samples of the multicarrier signal. The

OFDM signal can be described as a set of closely spaced frequency division multiplexing subcarriers where, in the frequency domain, each transmitted subcarrier, i.e. $e^{2\pi \jmath lk/K}$ for $l = 0, \ldots, K-1$, results in a sinc function spectrum. Even though the carrier signals overlap in frequency, they remain orthogonal in that at digital frequencies $w_k = 2\pi k/K$, the individual peaks of subcarriers all line up with the nulls of the other subcarriers. A

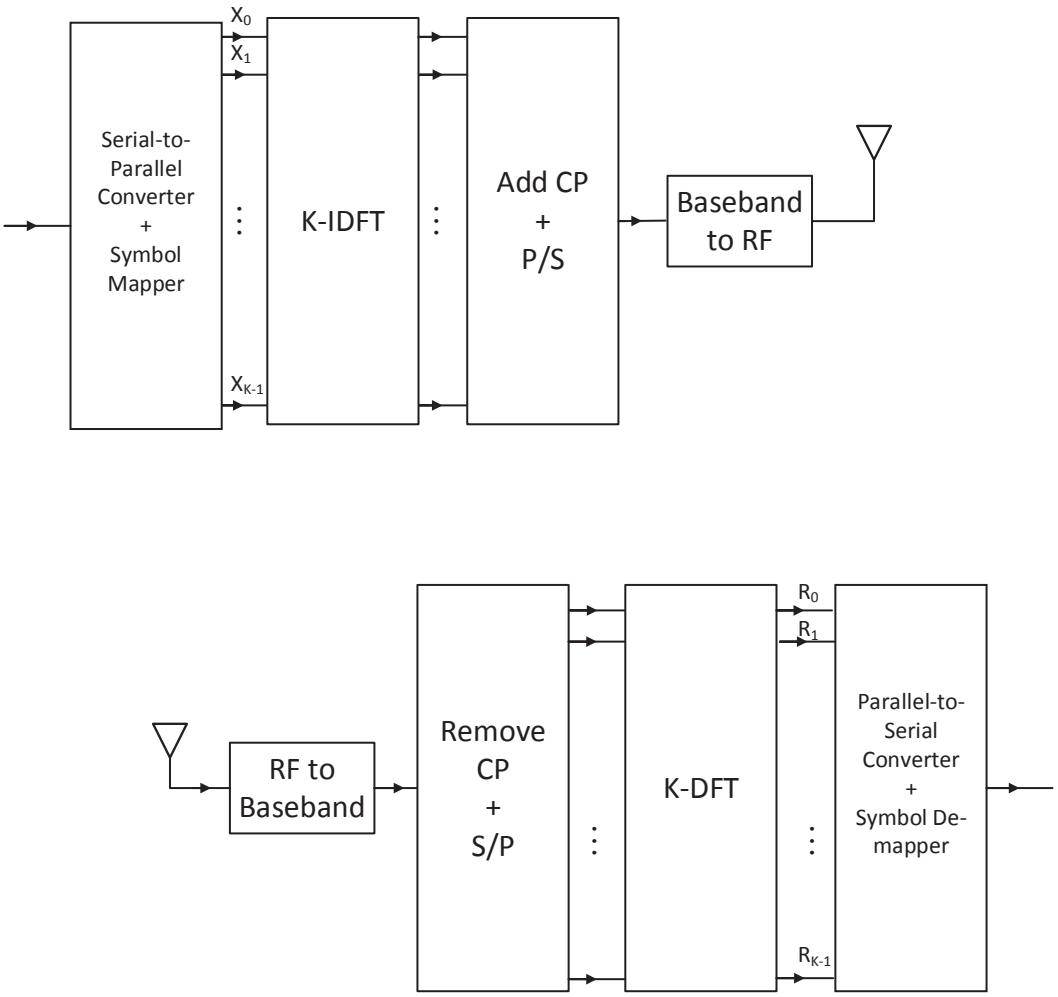

Fig. 3.4 Schematic representation of OFDM transceiver

cyclic prefix (CP) is added at the beginning of the OFDM symbol, which is a copy of the last L_{CP} samples from $x(l)$. Specifically, the resulting time samples after serial-to-parallel

conversion with length $K + L_{CP} - 1$, are given by [42]:

$$\tilde{x}(l) = [x(K - L_{CP}), ..., x(K-2), x(K-1), x(0), x(1), ..., x(K-1)] \tag{3.4}$$

where $l = -L_{CP}, \ldots, K-1$. The CP serves as a guard band to minimize the ISI between the different transmitted OFDM data symbols, as caused by the delay spread in the radio channel. Finally, the discrete-time baseband signal $\tilde{x}(l)$ is converted to an analog passband signal for transmission, via analog pulse-shaping and RF up-conversion.

Let $r(l)$ denote the baseband signal at the OFDM receiver front-end after RF down-conversion and sampling. in the receiver side, the first step is to remove the CP prefix consisting of the first L_{CP} samples of $r(l)$. The resulting K time samples are converted to a parallel stream via a serial-to-parallel converter. The signal $r_j(l)$ is then mapped to the frequency domain by applying a K-point DFT operation. Specifically, the resulting symbols R_k, corresponding to carrier index k, is formulated as:

$$R_k = \sum_{l=0}^{K-1} r(l) \mathrm{e}^{-2\pi \jmath lk/K} \tag{3.5}$$

where the index $k = 0, 1, ..., K-1$. Each output symbol is passed through a corresponding subchannel equalizer and QAM detector (not shown), Subsequently, the final bit stream is obtained after parallel-to-serial conversion.

3.3 UFMC

UFMC has recently attracted researcher's attention due to its higher spectral efficiency and reduced intercarrier interference (ICI). In UFMC, a filtering operation is applied, unlike OFDM, to a group of consecutive subcarriers to minimize the potential interference from subcarriers of adjacent subbands. In the recent literature, slightly different implementations of the UFMC concept have been proposed [32–34]. The UFMC transceiver model that will be used in our work follows that of [32].

3.3.1 UFMC Operation

As seen from Fig. 3.5, at the transmitter, a group of K incoming complex data symbols are mapped into B subbands with index $j = 1, \ldots, B$, where each subband consists of $M = K/B$ tones with index $k = 0, \ldots, M-1$. The symbol affected to the k^{th} tone of the j^{th} subband is denoted as $X_{j,k}$. For each subband, the corresponding time domain symbols $x_j(l)$ are obtained by applying a K-point IDFT spreader on $X_{j,k}$. More specifically, the group of tones in the j^{th} subband is offset by inserting θ_j zeros at the beginning; similarly, zeros are inserted at the end to account for unallocated subcarriers. In effect, this operation can be expressed as [32]:

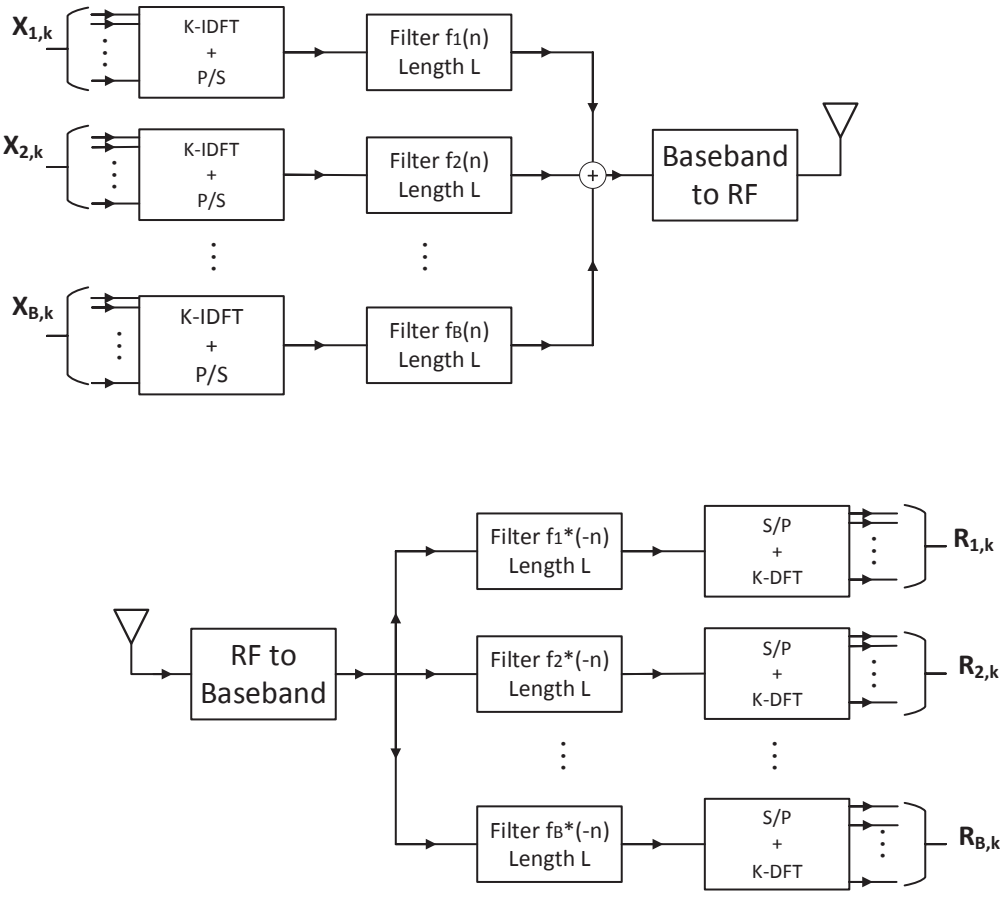

Fig. 3.5 Schematic representation of UFMC transceiver

$$x_j(l) = \frac{1}{K} \sum_{k=0}^{M-1} X_{j,k} \mathrm{e}^{2\pi \jmath l(k+\theta_j)/K} \tag{3.6}$$

where the index $l = 0, ..., K-1$ and $\theta_j = (j-1)M$. Each subband sequence $x_j(l)$ is passed through a corresponding finite impulse response (FIR) filter $f_j(l)$ of length L to reduce out-of-band leakage. Filter $f_j(l)$ is modulated to the proper frequency by multiplying a prototype impulse response $f(l)$ with an exponential sequence, that is: $f_j(l) = f(l)\mathrm{e}^{2\pi \jmath l(\theta_j+(M-1)/2)/K}$. In this work, similar to [32], $f(l)$ is obtained from a Dolph-Chebyshev (DC) window with adjustable sidelobe attenuation, as explained in subsection 3.3.2. The output of the j^{th} subband after FIR filtering is expressed as:

$$y_j(l) = x_j(l) * f_j(l) = \sum_{l'=0}^{K-1} x_j(l') f_j(l - l') \tag{3.7}$$

where $*$ denotes the discrete-time convolution and the index $l = 0, \ldots, K + L - 2$. The different subband signals $y_j(l)$ are then summed, resulting into

$$y(l) = \sum_{j=1}^{B} y_j(l) \tag{3.8}$$

Finally, the discrete-time baseband signal $y(l)$ is converted to an analog passband signal for transmission, via analog pulse-shaping and RF up-conversion.

Let $r(l)$ denote the baseband signal at the UFMC receiver front-end after RF down-conversion and sampling. For each one of the B subbands, the received signal $r(l)$ is convolved with the time reversal and complex conjugate of the corresponding subband filter $f_j(l)$. The resulting time-domain signal, denoted as $r_j(l)$, can be expressed as:

$$r_j(l) = r(l) * f_j^*(-l) = \sum_{l'=0}^{K+L-2} r(l') f_j^*(l' - l) \tag{3.9}$$

where only the samples with index $l = 0, ..., K-1$ are retained [14]. For each subband, the signal $r_j(l)$ is mapped to the frequency domain by applying a K-point DFT despreading operation. Specifically, the estimated symbol corresponding to the k^{th} tone of the j^{th}

subband is expressed as:

$$R_{j,k} = \sum_{l=0}^{K-1} r_j(l) \mathrm{e}^{-2\pi \jmath l(k+\theta_j)/K} \tag{3.10}$$

where the index $k = 0, \ldots, M-1$.

3.3.2 FIR Filter Design

The FIR prototype filter $f(l)$ used in our work is a discrete-time FIR DC filter similar to [32]. These filters are parameterizable in their shape to maximize the side lobe attenuation given a main lobe width. Unlike most windows, the DC window is defined in terms of its frequency response and is designed using the frequency sampling method. That is, it is constructed from the frequency domain by uniformly taking samples of the windows Fourier transform [44, 45]. The DC window is defined in the frequency domain by the following expression [45, 46]:

$$F(\omega) = \frac{C_{L-1}(x_0 \cos(\omega/2)))}{C_{L-1}(x_0)}, \quad 0 \leq \omega < 2\pi \tag{3.11}$$

where $x_0 > 1$ is an adjustable parameter and $C_m(x)$ are the well-known Chebyshev polynomials of the first kind that were first used by Dolph in 1946 to solve the problem of designing a radio antenna having optimal directional characteristics [47]. These polynomials can be defined by the following equations [48]:

$$C_m(x) = \begin{cases} \cos(m \cos^{-1}(x)), & \text{for } |x| \leq 1 \\ \cosh(m \cosh^{-1}(x)), & \text{for } x \geq 1 \\ (-1)^m \cosh(m \cosh^{-1}(-x)), & \text{for } x \leq -1 \end{cases} \tag{3.12}$$

We define ω_s as the stop-band frequency such that:

$$x_0 \cos(\omega_s/2) = 1 \tag{3.13}$$

and r is defined as the stop-band ripple such that, in the pass-band, as ω varies from 0 to w_s, $F(\omega)$ falls from 1 to $r = 1/C_{L-1}(x_0)$. $F(\omega)$ oscillates from $\pm r$ in the stop-band (i.e. for

$\omega_s \leq \omega \leq \pi$) [46]. The form of $F(\omega)$ follows that of the magnitude response of a lowpass filter. Following the sampling operation, at sampled frequencies $\omega_k = 2\pi k/L$, the L^{th} order DC window in the frequency domain can be expressed as [46]:

$$F(w_k) = \frac{C_{L-1}(x_0 \cos(\pi k/L)))}{C_{L-1}(x_0)} \tag{3.14}$$

where index $k = -(\frac{L}{2}-1), \ldots, -1, 0, 1, \ldots, \frac{L}{2}-1$ assuming L is even. Following this, the coefficients of the discrete-time DC filter's impulse response $f(l)$ are obtained by taking the IDFT of F_k and scaling the result to have a peak value of 1. This can be formulated as:

$$f(l) = \sum_{k=-(\frac{L}{2}-1)}^{\frac{L}{2}-1} F_k \mathrm{e}^{2\pi \jmath lk/L} \tag{3.15}$$

where index $l = -(\frac{L}{2}-1), \ldots, -1, 0, 1, \ldots, \frac{L}{2}-1$. Due to the symmetry in $F(\omega)$, we assume that the window $f(l)$ has real-valued coefficients. Consequently, we can also write $f(l)$ as [46]:

$$f(l) = \frac{1}{L}\left(F_0 + 2\sum_{k=1}^{\frac{L}{2}-1} \mathrm{Re}(F_k \mathrm{e}^{2\pi \jmath lk/L})\right) \tag{3.16}$$

$$= \frac{1}{L}\left(1 + 2r \sum_{k=1}^{(L-1)/2} C_{L-1}\big(x_0 \cos(\frac{\pi k}{L})\big) \cos(\frac{2l\pi k}{L})\right) \tag{3.17}$$

For the UFMC receiver, we use the DC window directly as the prototype low pass filter. In the design, the filter order L and maximum amplitude r in the stop-band are chosen. From this, the width of the main-lobe $2\omega_s$ can be computed as:

$$\omega_s = 2\cos^{-1}(\frac{1}{x_0}) \tag{3.18}$$

where

$$x_0 = \cosh(\frac{1}{L-1}\cosh^{-1}(\frac{1}{r})) \tag{3.19}$$

The main-lobe width of the resulting window is minimum for the given filter order L and ripple ratio r. The magnitude response (in dB) of F_k is shown in Fig. 3.6 for $L = 74$ and -120dB minimum attenuation in the stop-band ($r = 10^{-6}$). Since the side-lobes are of equal height, they are often called ripple in the stop-band. Given a window length L, the larger the main-lobe width is, the smaller the stop-band ripple specification. The window

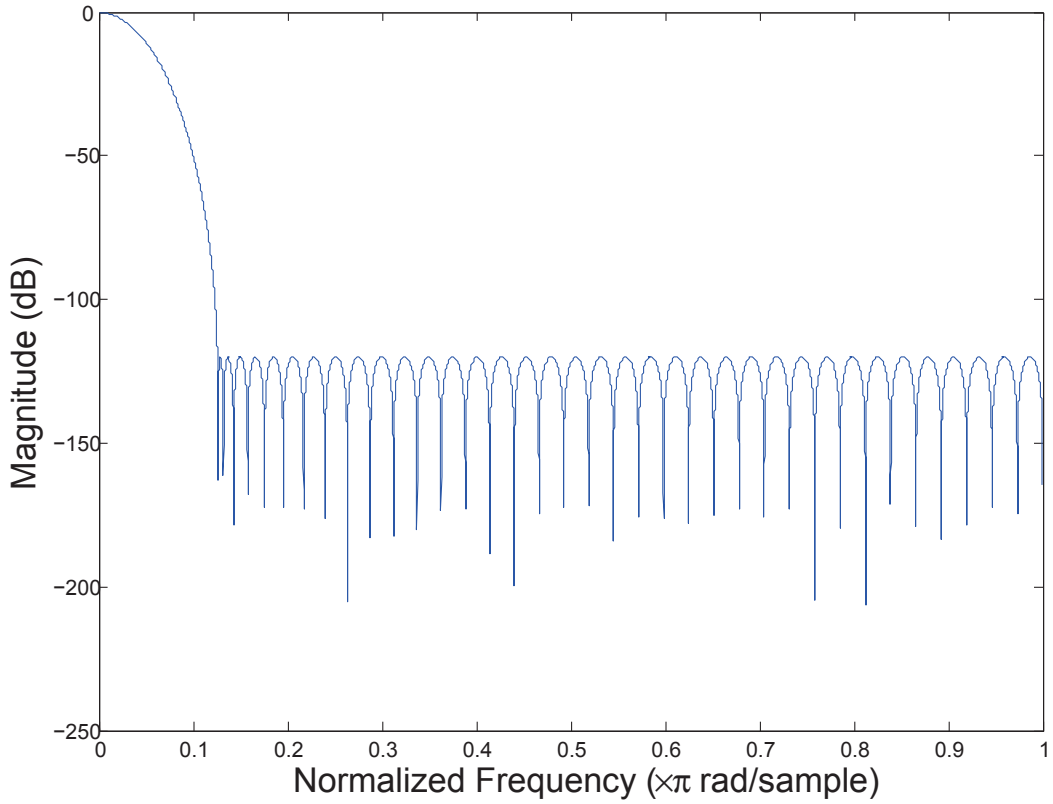

Fig. 3.6 Magnitude response of Dolph-Chebyshev window for $L = 74$ and -120dB side-lobe level

is made causal such that the index $l = 0, \ldots, L-1$ by time-shifting the window by half a window length. The causal discrete-time window $f(l)$ for $L = 74$ and -120dB ($r = 10^{-6}$) stop-band ripple is plotted in Fig. 3.7.

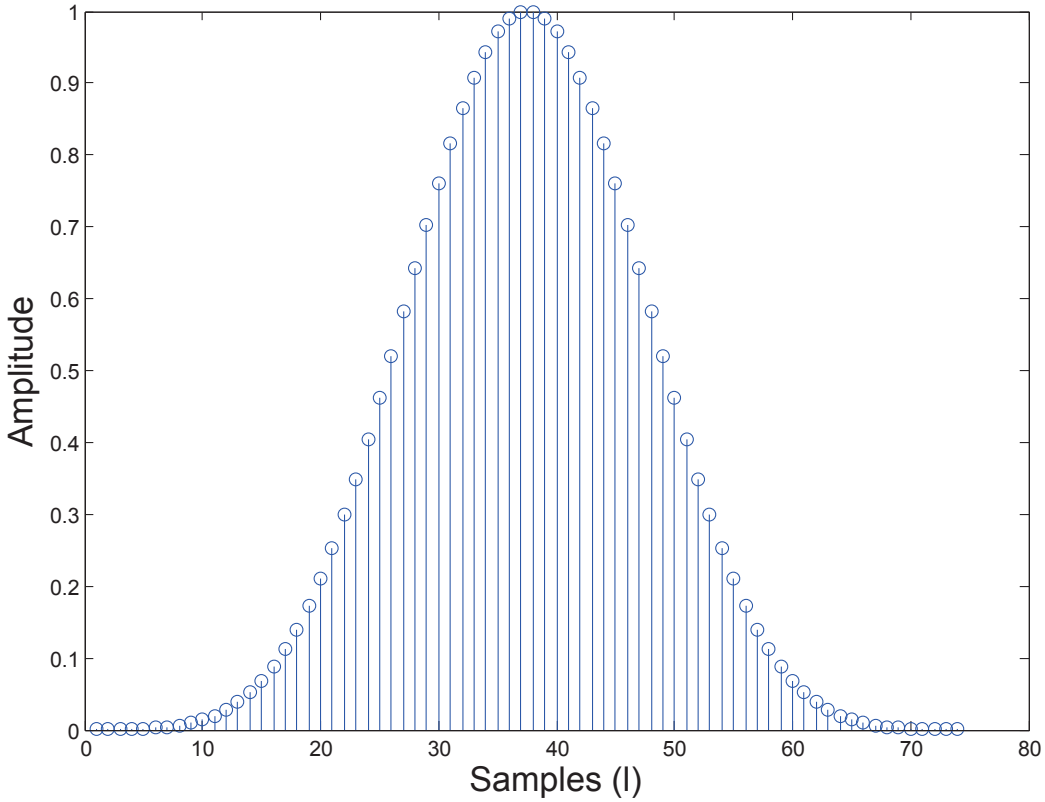

Fig. 3.7 Dolph-Chebyshev window for $L = 74$ and -120dB side-lobe level

Chapter 4

Multicarrier Wideband Spectrum Sensing with UFMC

In this chapter, we incorporate the optimal non-coherent Rao detector for non-Gaussian noise environments into the UFMC scheme. For the sake of comparison, we also discuss the incorporation the Rao detector into OFDM. We first describe the model considered in this work for wideband spectrum sensing. Then, we present the test statistics for the UFMC and OFDM based receiver with Rao detection in non-Gaussian noise.

4.1 Wideband Spectrum Sensing Model

For the wideband spectrum sensing model, we consider a multipath fading environment where $h(l)$ represents the baseband equivalent discrete-time impulse response of the radio channel between the PU and SU. That is, the signal at the receiver front-end of the SU can be written as:

$$r(l) = h(l) * y(l) + w(l) \tag{4.1}$$

where $y(l)$ is the PU signal component and $w(l)$ is the additive complex white noise with zero mean and variance σ_w^2. We note that the specific transmission scheme for the PU signal component $y(l)$ need not be known by the SU; that is, the PU may not necessarily employ UFMC or OFDM for transmission. We assume that the unknown PU signal component $y(l)$ and additive GGD noise $w(l)$ are statistically independent of each other. We also

assume that the complex channel $h(l)$ between the PU and SU is slowly fading such that it can be assumed to remain constant during each sensing operation period.

4.2 Integration into OFDM

Following Section 3.2, for a SU equipped with a OFDM-based receiver, the received signal in the frequency domain, on the k^{th} tone of the j^{th} subband, is then given by $R_{j,k}$ in (3.5). On this basis, a schematic representation of OFDM-based wideband spectrum sensing is shown in Fig. 4.1. For a matter of consistency and comparison with UFMC, we also

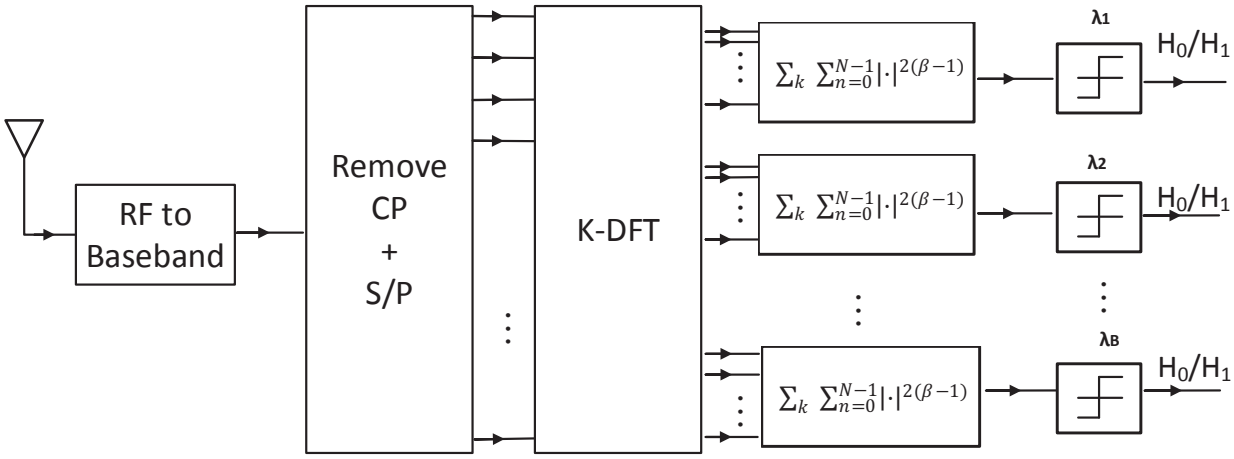

Fig. 4.1 Schematic representation of OFDM-based wideband spectrum sensing

assume, that the detection is made on a "per subband" basis, where a subband consists of a group of M contiguous tones or subcarriers. We test the following binary hypotheses to decide whether the j^{th} subband, which consists of M tones with index $k = 0, 1, \ldots, M-1$, is accessible or not:

$$H_{0,j} : R_{j,k}(n) = W_{j,k}(n) \tag{4.2}$$

$$H_{1,j} : R_{j,k}(n) = H_{j,k} Y_{j,k}(n) + W_{j,k}(n) \tag{4.3}$$

where $n = 0, 1, \ldots, N-1$, and N is the total number of OFDM symbols in the given observation window. Here, $R_{j,k}(n)$ denotes the n^{th} estimated symbol on the k^{th} tone of the j^{th} subband, $H_{j,k}$ is the corresponding complex channel gain between the PU and SU,

$Y_{j,k}(n)$ is the unknown PU signal component, and $W_{j,k}(n)$ is a GGD noise with zero mean and variance σ_w^2.

For each subband j, we compute the test statistic of the Rao detector over an interval of N symbols. The test statistic of the Rao detector for the j^{th} subband is obtained as the sum of the contributions from each symbol affected to the various tones with index k in that subband, assuming independent symbol sequences. Specifically, it is formulated as:

$$T_R\{R_{j,k}(n)\} = \phi(\beta) \sum_{k=0}^{M-1} \sum_{n=0}^{N-1} (|R_{j,k}^{\mathrm{Re}}(n)|^{2(\beta-1)} + |R_{j,k}^{\mathrm{Im}}(n)|^{2(\beta-1)}) \tag{4.4}$$

where $R_{j,k}^{\mathrm{Re}}(n)$ and $R_{j,k}^{\mathrm{Im}}(n)$ represent the real and imaginary parts of $R_{j,k}(n)$. The test statistic for the energy detector is formulated as:

$$T_E\{R_{j,k}(n))\} = \sum_{k=0}^{M-1} \sum_{n=0}^{N-1} |R_{j,k}(n)|^2 \tag{4.5}$$

The decision rule is chosen as:

$$T_R\{R_{j,k}(n)\} \underset{H_{0,j}}{\overset{H_{1,j}}{\gtrless}} \lambda_j \tag{4.6}$$

where λ_j is the decision threshold for the j^{th} subband.

4.3 Integration into UFMC

A schematic representation of UFMC-based wideband spectrum sensing is shown in Fig. 4.2. Following Section 3.3, for a SU equipped with a UFMC-based receiver, the discrete-time signal $r(l)$ at the baseband front-end is filtered by subband filters $f_j^*(-l)$ for $j = 1, \ldots, B$. In the frequency domain, following the despreading operation, the received signal on the k^{th} tone of the j^{th} subband is then given by $R_{j,k}$ in (3.10).

We test the following binary hypotheses to decide whether the j^{th} subband, which

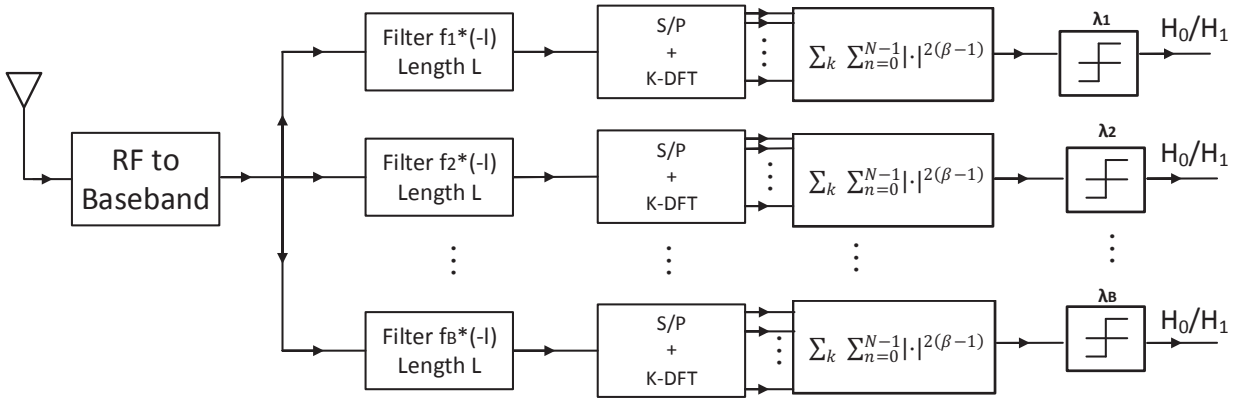

Fig. 4.2 Schematic representation of UFMC-based wideband spectrum sensing

consists of M tones with index $k = 0, 1, \ldots, M-1$, is accessible or not:

$$H_{0,j} : R_{j,k}(n) = W_{j,k}(n) \tag{4.7}$$

$$H_{1,j} : R_{j,k}(n) = H_{j,k} F^*_{j,k}(n) Y_{j,k}(n) + W_{j,k}(n) \tag{4.8}$$

where $n = 0, 1, \ldots, N-1$, and N is the total number of UFMC symbols in the given observation window. Here, $R_{j,k}(n)$ denotes the n^{th} estimated symbol on the k^{th} tone of the j^{th} subband, $H_{j,k}$ is the corresponding complex channel gain between the PU and SU, $F^*_{j,k}(n)$ is the K-point DFT of $f^*_j(-n)$, $Y_{j,k}(n)$ is the unknown PU signal component, and $W_{j,k}(n)$ is a GGD noise with zero mean and variance σ^2_w. In practice, the Rao detector needs only to estimate the noise power σ^2_w and square magnitude of the complex channel gains $H_{j,k}$.

For each subband j, we compute the test statistic of the Rao detector over an interval of N symbols. Since a subband in UFMC consists of multiple tones or subcarriers, the test statistic for the j^{th} subband is obtained as the sum of the contributions from each symbol affected to the various tones with index k in that subband, assuming independent symbol sequences, and is formulated as in (4.4) and the decision rule is chosen as in (4.6).

For CR systems, the channel sensing mechanism needs to have a high spectral dynamic range in order to reliably detect available spectrum holes. That is, the receiver should be able to avoid interference from other signals within the channel for the reason that interference results in spectral estimates in the bands with low level energy to be greatly

biased. While OFDM is mostly used as a wideband channel sensing method for its simplicity of implementation, it suffers from a number of shortcomings that originate from the large sidelobes of the frequency response of the rectangular window filters that characterize each OFDM subband. The magnitude of the sidelobes determines the amount of leakage that each subband will receive from other parts of the spectrum. Such leakage is undesirable for CR applications. Hence, we propose using UFMC at the receiver with filtering, exhibiting a magnitude response with lower sidelobe levels than OFDM, to improve on the precision of the spectral estimates.

Indeed, by using a sensing system with subband filtering, the sidelobes of the filter associated with each subband can be made arbitrarily small by adjusting the filter length and stopband attenuation through the DC filter design presented in Section 3.3.2. Therefore, this will significantly reduce the spectral leakage from other parts of the spectrum improving the detection performance. Moreover, when transmitting data within the available subbands, the SU will be able to confine the spectral content winthin that subband more effectively recuding interference to other SUs and PUs.

Chapter 5

Simulation Results and Discussion

In this section, we first describe the methodology used to simulate the UFMC-based wideband system for PU detection. We then show the sidelobe behavior and symbol error rate for the UFMC and OFDM schemes to motivate the assumption that subband filtering improves spectral estimation and reduces interference with other SUs and PUs when transmitting within a spectrum hole. We obtain the ROC curves for UFMC-based receiver with the Rao detector and energy detector and compare them to that of the OFDM-based receiver with both detectors. We also evaluate the effect of the non-Gaussianity level (shaping factor β), SNR, and number of samples N in the observation window on the detection performance.

5.1 Methodology

We consider a wideband spectrum sensing system with a PU transmitting OFDM symbols over 256 tones each carrying random QPSK data symbols. For simplicity, the transmitted signal has unit power, that is $E[|y(l)|^2] = 1$. We assume that the PU and SU cover the same bandwidth, that is the SU is equipped with a UFMC-based receiver, also with $K = 256$ tones. The signal at the receiver front-end is filtered by $B = 8$ subband DC FIR filters of length $L = 74$ and with 35dB sidelobe attenuation. The filter coefficients $f(l)$ are chosen such that $\sum_{l=0}^{L-1} |f(l)|^2 = 1$. For the purpose of comparison, we also implement a system where the SU is equipped with an OFDM receiver with $K = 256$ tones.

The wireless fading channel, accounting for shadowing, refractions and reflections of the transmitted signal by surrounding obstacles is modeled as a tapped-delay line channel. This can be seen as an FIR filter with impulse response samples following the Rayleigh

distribution. More precisely, the Rayleigh fading channel impulse response is modeled as the sum of two uncorrelated real Gaussian random variables, which can be expressed as:

$$h(l) = h_I(l) + \jmath h_Q(l) \tag{5.1}$$

where $h_I(l)$ and $h_Q(l)$ represent the uncorrelated zero mean Gaussian sequences forming the real and imaginary parts of the channel taps. In our experiments, we assume a fading channel consisting of 5 channel taps that does not vary over one observation window of N multicarrier symbols. The channel impulse response is normalized such that its energy $\sum_{n=0}^{4} |h(l)|^2 = 1$.

The noise in (4.1) is modeled as GGD with zero mean, variance σ_w^2, and parameter β. The samples are generated using the following procedure [49]:

- simulating a Gamma random variable $Z \sim$ Gamma (a,b) with parameter $a = \beta^{-1}$ and $b = (A(\beta, \sigma_w^2))^{-\beta}$;
- applying the transformation $Y = Z^{1/\beta}$;
- setting $w(l)$ to $\pm Y$ with probability of 0.5.

Under the previous normalization assumptions for the PU signal and channel, the SNR in dB is given as:

$$\text{SNR} = -10 \log_{10}(\sigma_w^2) \tag{5.2}$$

At the receiver of the system, unless otherwise indicated, data are collected over $N = 25$ vector symbols. Comparison of the detection performance is performed over the second subband (i.e. $j = 2$) where interference from neighboring subbands is present. In this way, we can compare UFMC and OFDM in terms of their robustness to out-of-band interference. The performance of the various detection algorithms under comparison is evaluated in terms of the probability of detection P_d and the probability of false alarm P_{fa}, as shown through parametric ROC curves. The ROC curves are obtained through Monte-Carlo simulations over 10^4 independent runs.

5.2 SER Curves and Sidelobe Behavior for UFMC and OFDM

In this section we show SER curves and the sidelobe behavior for the UFMC and OFDM system in presence of non-Gausian noise impairments. We can demonstrate, through the sidelobe curves, that with the use of FIR filters in UFMC, we can potentially reduce the interference from other secondary users and we can get a better detection at the receiver. Moreover, we can show that SUs transmitting with UFMC over the spectrum holes will maintain a better performance for high data rate in terms of symbol error rate.

We first show, in 5.1, the sidelobe behavior of the second subband for the UFMC and OFDM receivers. As expected, with added subband filtering at the receiver, UFMC has a better out-of-band rejection due its lower sidelobes. OFDM has high sidelobe levels resulting from the rectangular window shape in the time domain. This would indicate that a SU equipped with a UFMC receiver will be able to better avoid the in-band interference from the other signals on the channel thereby increasing the PU detection performance. Moreover, an SU equipped with a UFMC transmitter will be able to confine more effectively its spectral content within the spectrum hole.

Fig. 5.2 shows the symbol error rate (SER) curves for a SU transmitting with UFMC and OFDM schemes over and additive white GGD noise channel with factor $\beta = 1.1$. We can see that a SU transmitting with UFMC will maintain a better SER performance than transmitting with OFDM. Specifically, for an SER performance of 10^{-3}, we observe an improvement of 1.5dB in the SNR.

5.3 ROC Curves for Rao and Energy Detectors in UFMC and OFDM

We now show the simulated ROC curves of the Rao and energy detectors when integrated in the UFMC system and the OFDM system in presence of non-Gaussian noise, where the Rayleigh fading channel model in (5.1) between the PU and SU is assumed.

It can be observed, from 5.3 that the Rao detector outperforms the energy detector when the background noise is non-Gaussian with $\beta = 1.1$, and this for both UFMC and OFDM receiver schemes. Indeed, given a P_{fa} of 0.1, there is a 55% increase of P_d for the Rao detector over the energy detector in the OFDM system and 37% in the UFMC scheme. Moreover, it can be seen that with the use of filters in the UFMC scheme, the SU detects

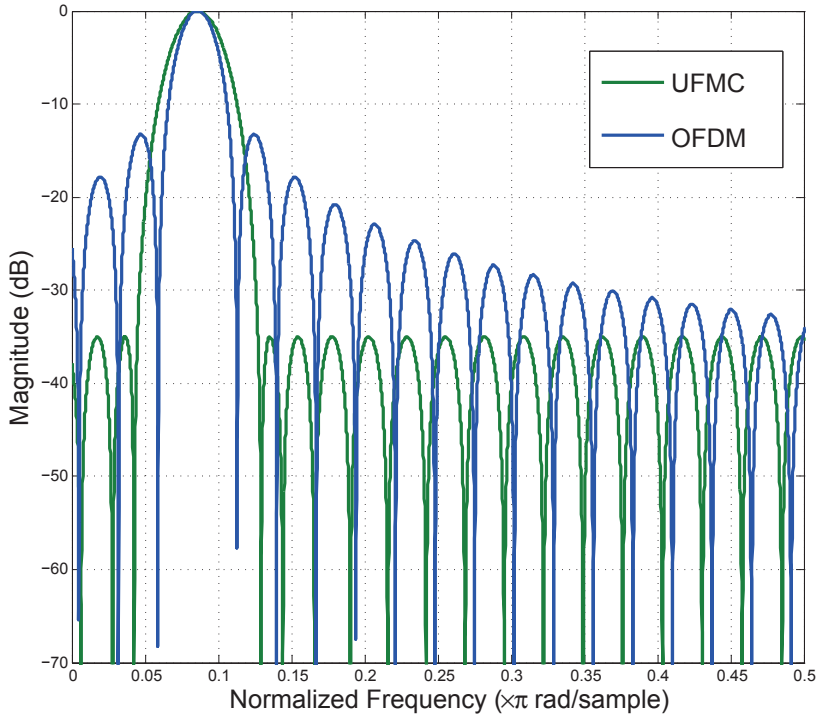

Fig. 5.1 Sidelobe behavior of UFMC and OFDM

better the presence of a PU in a given band over the OFDM scheme. We can observe from the figure that given a P_{fa} of 0.1, the Rao detector in the UFMC system surpasses the Rao detector in the OFDM system by 14%.

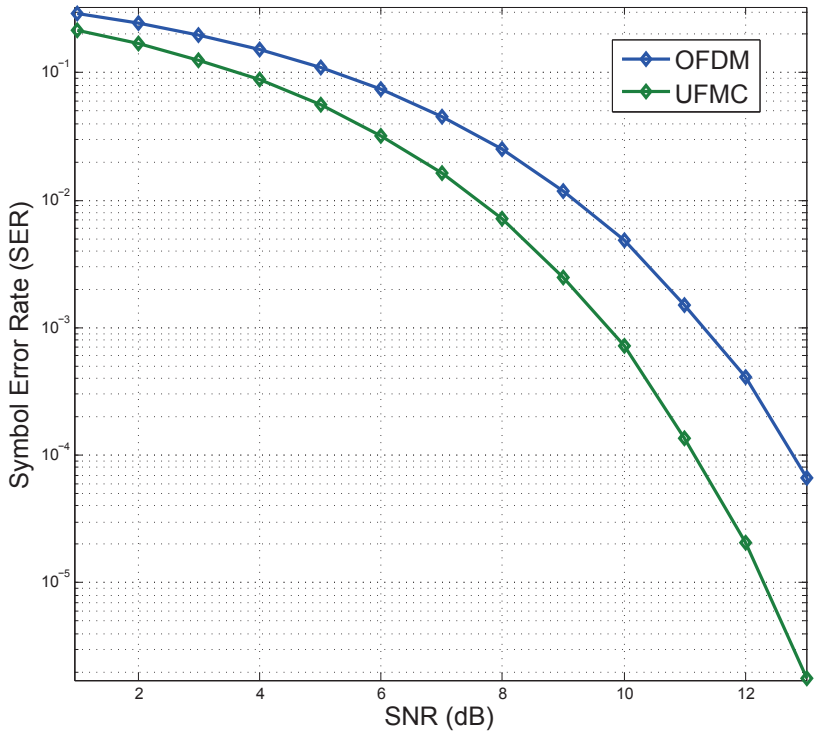

Fig. 5.2 SER for OFDM and UFMC in GGD noise environment for $\beta = 1.1$

Fig. 5.4 shows the effects of the noise shaping factor β on the ROC curves of the energy and Rao detectors integrated in the UFMC system. We can see that, as β decreases or the non-Gaussianity of the noise increases, the P_d rises. This is not the case for the energy detector, where as β decreases or the non-Gaussianity of the noise increases, the P_d drops. This means that SUs will be able to detect the PU signal more effectively, when using the Rao detector over the energy detector, in practical non-Gaussian noise environments which tend to exhibit probability density functions with tails decaying at lower rates than the traditional Gaussian density tails (i.e. shaping factor $\beta < 2$). Note that in generating them and other ROC curves, we assume that the value of the GGD noise shaping factor β is known at the receiver.

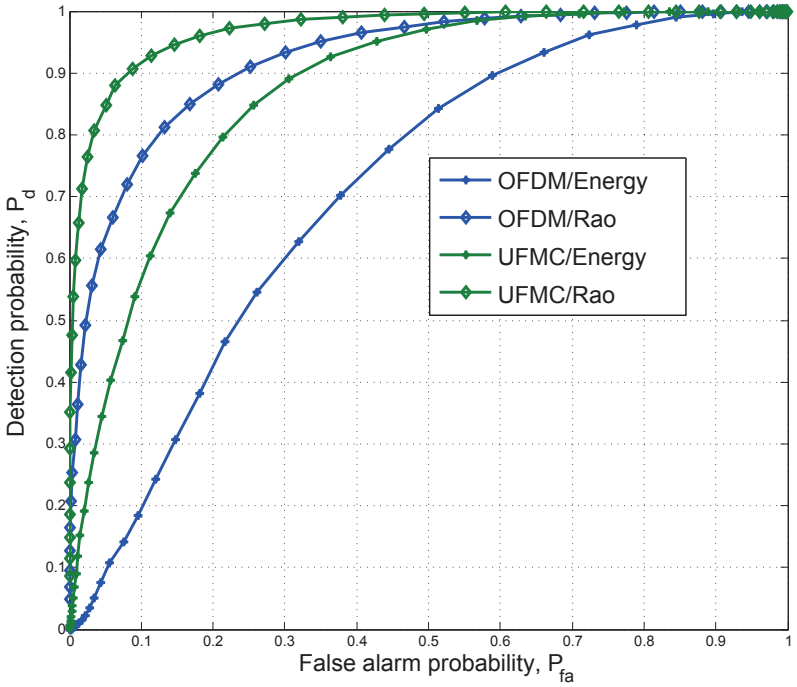

Fig. 5.3 ROC curves of the Energy and Rao detectors integrated in UFMC and OFDM for $\beta = 1.1$ and SNR = -10dB

In Fig. 5.5, the ROC curves of the Rao and energy detectors incorporated in the UFMC system for different SNRs are shown. As expected, the detection performance of the Rao detector is reduced as the SNR is reduced but is much better than with the energy detector for all values of SNR. This would indicate that the SU will be able to detect more effectively the PU with the Rao detector over the energy detector when non-Gaussian noise impairments are present and especially at low SNR.

In Fig. 5.6, the performances of the Rao and energy detectors integrated into UFMC versus the number of samples N in the observation window are shown for $\beta = 1.3$, and SNR $= -10$dB. It can be seen that, for the same probability of detection, the number of samples required by the Rao detector is lower than that of the energy detector. Alternatively, for the same number of observed samples N, the probability of detection for the Rao detector is greater than for the energy detector. We can also see that the the performance of the Rao detector increases as the number of samples in the observation window increases. The results presented in this section demonstrate the advantage of using the Rao detector integrated into UFMC when non-Gaussian noise is present. Compared to the en-

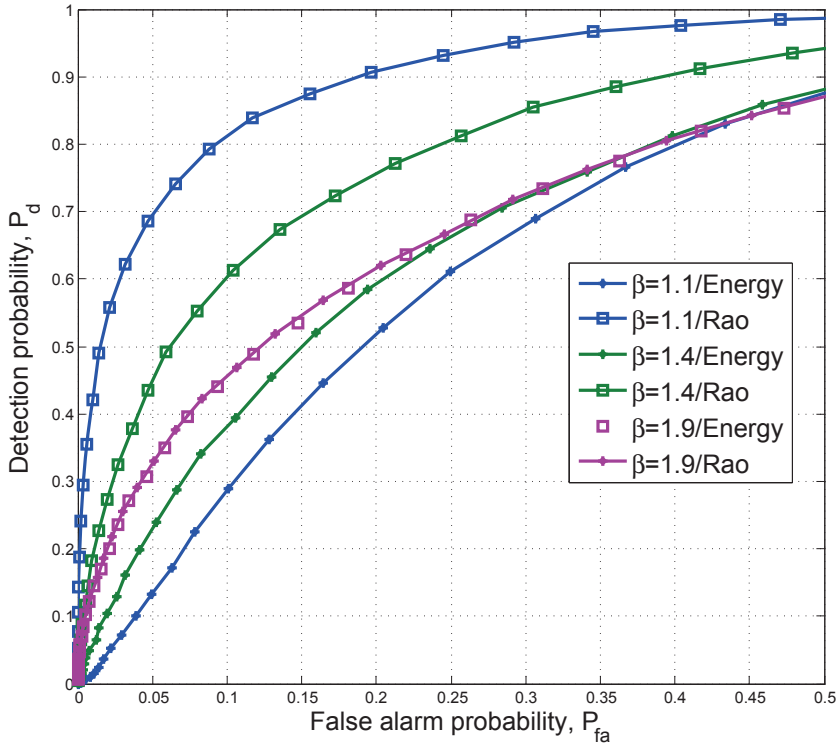

Fig. 5.4 Effect of GGD noise shaping factor β on ROC curve for Rao and energy detector integrated in UFMC for SNR = -20dB

ergy detector integrated into OFDM, UFMC achieves much better spectral dynamic range for any given noise with factor β. Through numerical results, we were able to establish the superior sensing performance of the Rao detector compared to the traditional energy detector contemporarily being used for cognitive radio applications.

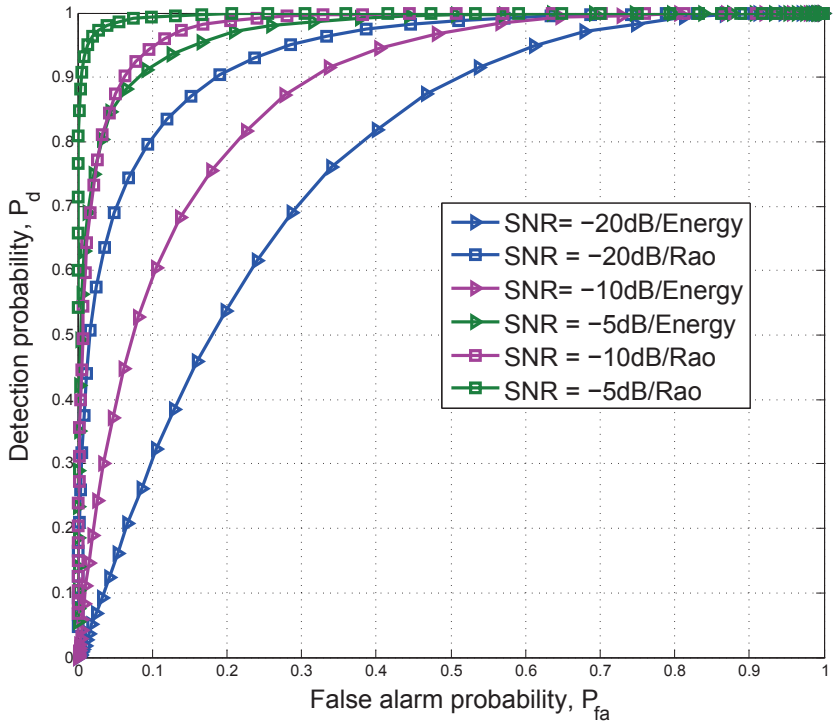

Fig. 5.5 Effect of SNR (dB) on ROC curve of the Rao detector integrated in UFMC and OFDM for $\beta = 1.1$

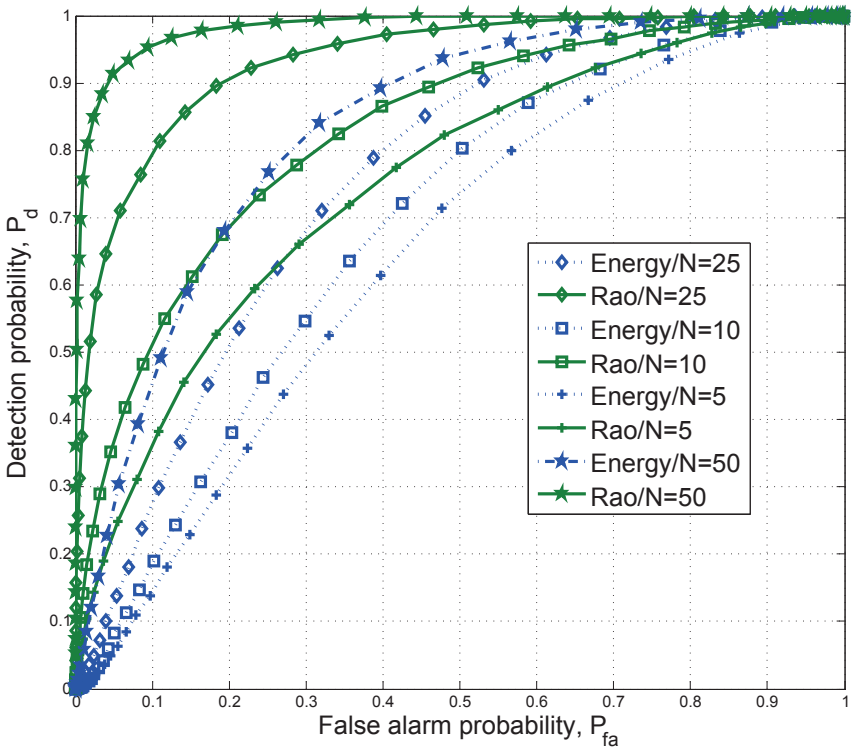

Fig. 5.6 Effect of total number of samples N in the observation window on ROC curve for Rao dector integrated in UFMC for SNR = -10dB and $\beta = 1.3$

Chapter 6

Conclusion and Future Work

This thesis addressed the problem of wideband spectrum sensing for cognitive radio applications. In particular, we considered the sensing task in a multicarrier framework and in scenarios where non-Gaussian impairments are present. The goal was to investigate the performance of the Rao-test based detector under non-Gaussian noise for wideband spectrum sensing incorporated into the UFMC modulation scheme envisaged for 5G systems. In this section, we present a summary of the work presented in this thesis followed by suggestions of some directions that may be considered for further work in this area.

6.1 Thesis Summary

In Chapter 1, a concise summary on the background and issues of wideband spectrum sensing for cognitive radios in non-Gaussian noise environments was initially presented. A literature survey on the topics related to the research conducted in this work, such as multicarrier modulation schemes and spectrum sensing techniques, was also presented.

In Chapter 2, selected spectrum sensing techniques for a wideband channel were covered. The chapter started with a formulation of the wideband CR spectrum sensing problem and the fundamentals of PU signal detection were presented. Then, detection algorithms based on PU cyclostationary features and matched filter detection were briefly outlined. Finally, techniques optimized for Gaussian and non-Gaussian noise, where no *a priori* knowledge of PU signal characteristics is needed, such as the energy and Rao detector were discussed in detail.

In Chapter 3, we delved on the topic of multicarrier modulation which serves as a basis

for wideband spectrum sensing. An overview of MCM was briefly covered. Then, the operation of the traditional OFDM system and recently introduced UFMC system were discussed.

In Chapter 4, the wideband spectrum sensing model of the Rao detector optimized for non-Gaussian noise environments intergated into the UFMC scheme was presented. For the sake of comparison, we also incorporated the Rao detector into the OFDM scheme. Specifically, we showed the test statistics for the UFMC and OFDM-based receiver with Rao detection in non-Gaussian noise.

In Chapter 5, the experiments used to simulate the UFMC-based wideband system for PU detection were described. It was shown, through ROC curves, that the Rao detector integrated in the UFMC system outperforms the traditional energy detector incorporated into OFDM in scenarios where non-Gaussian noise is present.

6.2 Future Work

This thesis showed ways to exploit multicarrier schemes with filtering in order to improve wideband channel spectrum sensing performance. However, there is room for further improvement to channel sensing techniques in the CR context. Possible directions for future work based on this thesis may include the following:

- It is possible to employ cooperative sensing as solution to overcome the effect of channel fading [1]. That is, collaborative CRs exploit spatial diversity in that each of them observes their received signal under independent fading, and then make a collaborative decision thereby increasing the probability of detection considerably. Specifically, a possible scenario is that CRs share information among each other and make their own decisions as to which part of the spectrum they can use

- It is also possible to have CRs equipped with multiple antennas such that the effect of fading in the channel between PU and SU can be reduced [50]. The cognitive SU is equipped with multiple antennas that will sense the PU, where each antenna experiences different fading, thereby offering several observations of the same signal in a similar fashion to collaborative sensing.

- One possible approach to improve the performance of wideband sensing is to perform a multiband joint detection of the PU signal, rather than processing one band at the

time. The spectrum sensing problem can be formulate as an optimization problem by combining test statistics from multiple subbands and performing an optimal joint detection, where the goal is to chose the decision threshold for the various subbands with the aim to maximize the aggregate opportunistic throughput of the CR system [24].

Appendix A

Derivation of Mean and Variance of T_E Under Gaussian Noise

In this appendix, we show the derivation of $E[T_E\{R_j(n)\}|H_{0,j}]$, $\text{Var}[T_E\{R_j(n)\}|H_{0,j}]$, $E[T_E\{R_j(n)\}|H_{1,j}]$ and $\text{Var}[T_E\{R_j(n)\}|H_{1,j}]$ under Gaussian noise.

A.1 Derivation of $E[T_E\{R_j(n)\}|H_{0,j}]$

$$\begin{aligned} E[T_E\{R_j(n)\}|H_{0,j}] &= E[\sum_{n=0}^{N-1} |W_j(n)|^2] \\ &= \sum_{n=0}^{N-1} E[|W_j(n)|^2] \end{aligned}$$

Using (2.22), we get that:

$$E[T_E\{R_j(n)\}|H_{0,j}] = N\sigma_w^2 \tag{A.1}$$

A.2 Derivation of $Var[T_E\{R_j(n)\}|H_{0,j}]$

$$\begin{aligned}\mathrm{Var}[T_E\{R_j(n)\}|H_{0,j}] &= E[T_E\{W_j(n)\}^2] - E[T_E\{W_j(n)\}]^2 \\ &= \sum_{n=0}^{N-1}\sum_{m=0}^{N-1} E[|W_j(n)|^2|W_j(m)|^2] - N^2\sigma_w^4 \end{aligned} \tag{A.2}$$

Assuming the noise samples $W_j(n)$ are independent and identically distributed and using (2.22), we get that:

$$\sum_{n=0}^{N-1}\sum_{m=0}^{N-1} E[|W_j(n)|^2|W_j(m)|^2] = \begin{cases} 3N\sigma_w^4 & \text{for } n = m \\ N(N-1)\sigma_w^4 & \text{for } n \neq m \end{cases} \tag{A.3}$$

Following this, we obtain:

$$\begin{aligned}\mathrm{Var}[T_E\{R_j(n)\}|H_{0,j}] &= 3N\sigma_w^4 + N(N-1)\sigma_w^4 - N^2\sigma_w^4 \\ &= 2N\sigma_w^4 \end{aligned} \tag{A.4}$$

A.3 Derivation of $E[T_E\{R_j(n)\}|H_{1,j}]$

$$\begin{aligned}E[T_E\{R_j(n)\}|H_{1,j}] &= E[\sum_{n=0}^{N-1} |H_jS_j(n) + W_j(n)|^2] \\ &= \sum_{n=0}^{N-1} E[|H_jS_j(n) + W_j(n)|^2] \\ &= N\Big(E[|H_jS_j(n)|^2] \\ &\quad + 2|H_j|E[|S_j(n)|]E[|W_j(n)|] + E[|W_j(n)|^2]\Big) \end{aligned} \tag{A.5}$$

Assuming the noise samples $W_j(n)$ have zero mean and are independent from the PU signal $S_j(n)$, we get that:

$$E[T_E\{R_j(n)\}|H_{1,j}] = N(|H_j|^2 + \sigma_w^2) \tag{A.6}$$

A.4 Derivation of $Var[T_E\{R_j(n)\}|H_{1,j}]$

$$\begin{aligned}\mathrm{Var}[T_E\{R_j(n)\}|H_{1,j}] &= E[T_E\{R_j(n)\}^2] - E[T_E\{R_j(n)\}]^2 \\ &= E[T_E\{H_jS_j(n) + W_j(n)\}^2] - N^2(|H_j|^2 + \sigma_w^2)^2 \\ &= \sum_{n=0}^{N-1}\sum_{m=0}^{N-1} E[|H_jS_j(n) + W_j(n)|^2|H_jS_j(m) + W_j(m)|^2] \\ &\quad - N^2(|H_j|^2 + \sigma_w^2)^2 \end{aligned} \tag{A.7}$$

Using (A.6), we get that:

$$\begin{aligned}&\sum_{n=0}^{N-1}\sum_{m=0}^{N-1} E[|H_jS_j(n) + W_j(n)|^2|H_jS_j(m) + W_j(m)|^2] \\ &\quad = \begin{cases} \sum_{n=0}^{N-1} E[|H_jS_j(n) + W_j(n)|^4] & \text{for } n = m \\ N(N-1)(|H_j|^2 + \sigma_w^2)^2 & \text{for } n \neq m \end{cases}\end{aligned} \tag{A.8}$$

Following this, we obtain:

$$\begin{aligned}\mathrm{Var}[T_E\{R_j(n)\}|H_{1,j}] &= \sum_{n=0}^{N-1} E[|H_jS_j(n) + W_j(n)|^4] \\ &\quad - N(|H_j|^2 + \sigma_w^2)^2 \end{aligned} \tag{A.9}$$

Following this, we obtain:

$$\begin{aligned}\mathrm{Var}[T_E\{R_j(n)\}|H_{1,j}] &= \sum_{n=0}^{N-1} E[|H_jS_j(n) + W_j(n)|^4] \\ &\quad - N(|H_j|^2 + \sigma_w^2)^2 \end{aligned} \tag{A.10}$$

Under the low SNR assumption, we can assume that $|S_j(n)| \ll |W_j(n)|$. Hence, we can approximate $E[|H_jS_j(n) + W_j(n)|^4]$ by using its Taylor series expansion around $W_j(n)$ and

ignoring higher-order terms [22]. Following this operation, we obtain:

$$\begin{aligned} E[|H_j S_j(n) + W_j(n)|^4] &\approx E[|W_j(n)|^4] + 4E[|H_j S_j(n)|^2]E[|W_j(n)|^2] \\ &= 3\sigma_w^4 + 4|H_j|^2\sigma_w^2 \end{aligned} \tag{A.11}$$

Finally, we have:

$$\begin{aligned} \mathrm{Var}[T_E\{R_j(n)\}|H_{1,j}] &= 3N\sigma_w^4 + 4N|H_j|^2\sigma_w^2 - N(|H_j|^2 + \sigma_w^2)^2 \\ &= N\Big[2\sigma_w^4 + 2|H_j|^2\sigma_w^2 - |H_j|^4\Big] \end{aligned} \tag{A.12}$$

Appendix B

Derivation of Mean and Variance of T_E Under GGD Noise

In this appendix, we show the derivation of $E[T_E\{R_j(n)\}|H_{0,j}]$, $\text{Var}[T_E\{R_j(n)\}|H_{0,j}]$, $E[T_E\{R_j(n)\}|H_{1,j}]$, and $\text{Var}[T_E\{R_j(n)\}|H_{1,j}]$ under GGD noise.

B.1 Derivation of $E[T_E\{R_j(n)\}|H_{0,j}]$

$$\begin{aligned} E[T_E\{R_j(n)\}|H_{0,j}] &= E[\sum_{n=0}^{N-1} |W_j(n)|^2] \\ &= \sum_{n=0}^{N-1} E[|W_j(n)|^2] \end{aligned}$$

Using (2.31), we get that:

$$E[T_E\{R_j(n)\}|H_{0,j}] = N\sigma_w^2 \tag{B.1}$$

B.2 Derivation of $Var[T_E\{R_j(n)\}|H_{0,j}]$

$$\begin{aligned}\mathrm{Var}[T_E\{R_j(n)\}|H_{0,j}] &= E[T_E\{W_j(n)\}^2] - E[T_E\{W_j(n)\}]^2 \\ &= \sum_{n=0}^{N-1}\sum_{m=0}^{N-1} E[|W_j(n)|^2|W_j(m)|^2] - N^2\sigma_w^4 \end{aligned} \tag{B.2}$$

Assuming the noise samples $W_j(n)$ are independent and identically distributed and using (2.31), we get that:

$$\sum_{n=0}^{N-1}\sum_{m=0}^{N-1} E[|W_j(n)|^2|W_j(m)|^2] = \begin{cases} N\frac{\Gamma(1/\beta)}{\Gamma(3/\beta)^2}\Gamma(5/\beta)\sigma_w^4 & \text{for } n = m \\ N(N-1)\sigma_w^4 & \text{for } n \neq m \end{cases} \tag{B.3}$$

Following this, we obtain:

$$\begin{aligned}\mathrm{Var}[T_E\{R_j(n)\}|H_{0,j}] &= N\frac{\Gamma(1/\beta)}{\Gamma(3/\beta)^2}\Gamma(5/\beta)\sigma_w^4 + N(N-1)\sigma_w^4 - N^2\sigma_w^4 \\ &= N\sigma_w^4\Big(\frac{\Gamma(1/\beta)}{\Gamma(3/\beta)^2}\Gamma(5/\beta) - 1\Big) \end{aligned} \tag{B.4}$$

B.3 Derivation of $E[T_E\{R_j(n)\}|H_{1,j}]$

$$\begin{aligned}E[T_E\{R_j(n)\}|H_{1,j}] &= E[\sum_{n=0}^{N-1}|H_jS_j(n) + W_j(n)|^2] \\ &= \sum_{n=0}^{N-1} E[|H_jS_j(n) + W_j(n)|^2] \\ &= N\Big(E[|H_jS_j(n)|^2] \\ &\quad + 2|H_j|E[|S_j(n)|]E[|W_j(n)|] + E[|W_j(n)|^2]\Big) \end{aligned} \tag{B.5}$$

Assuming the noise samples $W_j(n)$ have zero mean and are independent with PU signal $S_j(n)$, we get that:

$$E[T_E\{R_j(n)\}|H_{1,j}] = N(|H_j|^2 + \sigma_w^2) \tag{B.6}$$

B.4 Derivation of $Var[T_E\{R_j(n)\}|H_{1,j}]$

$$\begin{aligned}\mathrm{Var}[T_E\{R_j(n)\}|H_{1,j}] &= E[T_E\{R_j(n)\}^2] - E[T_E\{R_j(n)\}]^2 \\ &= E[T_E\{H_jS_j(n) + W_j(n)\}^2] - N^2(|H_j|^2 + \sigma_w^2)^2 \\ &= \sum_{n=0}^{N-1}\sum_{m=0}^{N-1} E[|H_jS_j(n) + W_j(n)|^2|H_jS_j(m) + W_j(m)|^2] \\ &\quad - N^2(|H_j|^2 + \sigma_w^2)^2 \end{aligned} \tag{B.7}$$

Using (B.6), we get that:

$$\begin{aligned}&\sum_{n=0}^{N-1}\sum_{m=0}^{N-1} E[|H_jS_j(n) + W_j(n)|^2|H_jS_j(m) + W_j(m)|^2] \\ &\quad = \begin{cases} \sum_{n=0}^{N-1} E[|H_jS_j(n) + W_j(n)|^4] & \text{for } n = m \\ N(N-1)(|H_j|^2 + \sigma_w^2)^2 & \text{for } n \neq m \end{cases}\end{aligned} \tag{B.8}$$

Following this, we obtain:

$$\begin{aligned}\mathrm{Var}[T_E\{R_j(n)\}|H_{1,j}] &= \sum_{n=0}^{N-1} E[|H_jS_j(n) + W_j(n)|^4] \\ &\quad - N(|H_j|^2 + \sigma_w^2)^2 \end{aligned} \tag{B.9}$$

Following this, we obtain:

$$\begin{aligned}\mathrm{Var}[T_E\{R_j(n)\}|H_{1,j}] &= \sum_{n=0}^{N-1} E[|H_jS_j(n) + W_j(n)|^4] \\ &\quad - N(|H_j|^2 + \sigma_w^2)^2 \end{aligned} \tag{B.10}$$

Under low SNR assumptions, we can assume that $|S_j(n)| \ll |W_j(n)|$. We can approximate $E[|H_jS_j(n) + W_j(n)|^4]$ by using its Taylor series expansion around $W_j(n)$ and ignoring

higher-order terms [22]. Following this operation, we obtain:

$$\begin{aligned} E[|H_j S_j(n) + W_j(n)|^4] &\approx E[|W_j(n)|^4] + 4E[|H_j S_j(n)|^2]E[|W_j(n)|^2] \\ &= \frac{\Gamma(1/\beta)}{\Gamma(3/\beta)^2}\Gamma(5/\beta)\sigma_w^4 + 4|H_j|^2\sigma_w^2 \end{aligned} \tag{B.11}$$

Finally, we have:

$$\begin{aligned} \mathrm{Var}[T_E\{R_j(n)\}|H_{1,j}] &= N\frac{\Gamma(1/\beta)}{\Gamma(3/\beta)^2}\Gamma(5/\beta)\sigma_w^4 + 4N|H_j|^2\sigma_w^2 - N(|H_j|^2 + \sigma_w^2)^2 \\ &= N\Big[\Big(\frac{\Gamma(1/\beta)}{\Gamma(3/\beta)^2}\Gamma(5/\beta) - 1\Big)\sigma_w^4 + 2|H_j|^2\sigma_w^2 - |H_j|^4\Big] \end{aligned} \tag{B.12}$$

Furthermore, the the mean and variance of $T_{E,j}$ under $H_{0,j}$ and $H_{1,j}$ subject to AWGN, as derived in appendix A, can also be obtained by setting the noise shaping factor β to 2 in the above equations.

References

[1] T. Yucek and H. Arslan, “A survey of spectrum sensing algorithms for cognitive radio applications," *Commun. Surveys Tuts*, vol. 11, no. 1, 2009, pp. 116-130.

[2] FCC Spectrum Policy Task Force ET Docket No. 02-135, Nov. 2002.

[3] D. Cabric, S.M. Mishra, D. Willkomm, R. Brodersen, A. Wolisz, “A Cognitive radio approach for usage of virtual unlicensed spectrum," in *Proc. 14th IST Mobile and Wireless Commun. Summit*, Dresden, Germany, June 2005.

[4] D. Bhargavi and C. R. Murthy, “Performance comparison of energy, matched-filter and cyclostationarity-based spectrum sensing," in *Proc. IEEE Workshop on Signal Advances in Wireless Commun.*, June 2010, pp. 1-5.

[5] J. G. Proakis and M. Salehi, *Digital Communications*, 5th ed. McGraw Hill, 2008.

[6] Z. Quan, S. Cui, H. V. Poor, and A. H. Sayed, “Collaborative wideband sensing for cognitive radios," *IEEE Signal Processing Magazine*, vol. 25, no. 6, pp. 60–73, Nov. 2008.

[7] B. Sklar, *Digital Communications: Fundamentals and Applications*, Prentice-Hall Inc., Englewood Cliffs New Jersey, 1988.

[8] J. K. Tugnait and G. Huang, “Cyclic autocorrelation based spectrum sensing in colored Gaussian noise," *in Proc. IEEE Wireless Commun. Netw. Conf.*, Paris, France, Apr. 1-4, 2012, pp. 731-736.

[9] K. Kim, I. A. Akbar, K. K. Bae, J. Um, C. M. Spooner., and J. H. Reed, “Cyclostationary approaches to signal detection and classification in cognitive radio," in *Proc.*

IEEE Int. Symp. New Frontiers in Dynamic Spectrum Access Networks, Apr. 2007, pp. 212–215.

[10] A. V. Dandawaté and G. B. Giannakis, “Statistical tests for presence of cyclostationarity," *IEEE Trans. Signal Processing*, vol. 42, pp. 2355–2369, Sept. 1994.

[11] J. Lundén, V. Koivunen, A. Huttunen, and H. V. Poor, “Collaborative cyclostationary spectrum sensing for cognitive radio systems," *IEEE Trans. Signal Processing*, vol. 57, pp. 4182–4195, Nov. 2009.

[12] S. Chaudhari, J. Lundén, and V. Koivunen, “Collaborative autocorrelation based spectrum sensing of OFDM signals in cognitive radios," in *Proc. Annu. Conf. Information Sciences and Systems (CISS)*, Princeton, NJ, Mar. 2008, pp. 191–196 .

[13] P. Qihang, Z. Kun, W. Jun, and L. Shaoqian, “A distributed spectrum sensing scheme based on credibility and evidence theory in cognitive radio context," in *Proc. IEEE Int. Symposium on Personal, Indoor and Mobile Radio Commun.*, Helsinki, Finland, Sept. 2006, pp. 1–5.

[14] M. Oner and F. Jondral, “Cyclostationarity based air interface recognition for software radio systems," in *Proc. IEEE Radio and Wireless Conf.*, Atlanta, Georgia, USA, Sept. 2004, pp. 263–266

[15] H. Urkowitz, “Energy detection of unknown deterministic signals," in *Proceedings of IEEE*, vol. 55, Apr. 1967, pp. 523–231.

[16] F. Digham, M.-S. Alouini and M. K. Simon, “On the energy detection of unknown signals over fading channels," in *Proc. of IEEE International Conference on Communications (ICC'03)*, May 2003, pp. 3575–3579.

[17] R. Umar, A. U. H. Sheikh, and M. Deriche, “Unveiling the hidden assumptions of energy detector based spectrum sensing for cognitive radios," *Commun. Surveys Tuts*, vol. 16, no. 2, 2014, pp. 713-728.

[18] D. Cabric, A. Tkachenko, and R. Brodersen, “Spectrum sensing measurements of pilot, energy, and collaborative detection," in *Proc. IEEE Military Commun. Conf.*, Washington, D.C., USA, Oct. 2006, pp. 1–7

[19] D. Cabric, S. Mishra, and R. Brodersen, “Implementation issues in spectrum sensing for cognitive radios," in *Proc. Asilomar Conf. on Signals, Systems and Computers*, vol. 1, Pacific Grove, California, USA, Nov. 2004, pp.772–776

[20] A. Ghasemi and E. Sousa, “Optimization of spectrum sensing for opportunistic spectrum access in cognitive radio networks," in *Proc. IEEE Consumer Commun. and Networking Conf.*, Las Vegas, Nevada, USA, Jan. 2007, pp. 1022–1026.

[21] S.A. Kassam, *Signal Detection in Non-Gaussian Noise*, Springer Verlag, 1988.

[22] X. Zhu, B. Champagne, and W. P. Zhu, “Rao test based cooperative spectrum sensing for cognitive radios in non-Gaussian noise," *Signal Process.*, vol. 97, Apr. 2014, pp. 183-194.

[23] H. Sun, A. Nallanathan, C.-X. Wang, and Y. Chen, “Wideband spectrum sensing for cognitive radio networks: A survey," *IEEE Wireless Commun.*, vol. 20, no. 2, Apr. 2013, pp. 74-81.

[24] Z. Quan, S. Cui, and A. Sayed, H. Poor, “Optimal multiband joint detection for spectrum sensing in cognitive radio networks," *IEEE Trans. on Signal Process. 57*, Mar. 2009, pp.1128-1140.

[25] K. Hossain, B. Champagne, and A. Assra, “Cooperative multiband joint detection with correlated spectral occupancy in cognitive radio networks," *IEEE Trans. on Signal Process.*, vol. 60, no. 5, May 2012, pp. 2682-2687.

[26] P. Banelli, S. Buzzi, G. Colavolpe, A. Modenini, F. Rusek, and A. Ugolini, “Modulation formats and waveforms for 5G networks: Who will be the heir of OFDM?: An overview of alternative modulation schemes for improved spectral efficiency," *IEEE Signal Process. Mag.*, vol. 31, no. 6, Nov. 2014, pp. 80-93.

[27] P. Amini, “Filterbank Multicarrier Techniques for Cognitive Radios,” Ph.D. dissertation, Dept. Elect. and Comp. Eng., Utah Univ., Utah, 2009.

[28] B. Farhang-Boroujeny, “Filter bank spectrum sensing for cognitive radios," in *IEEE Trans. Signal Processing*, vol. 56, pp. 1801–1811, May 2008.

[29] G. Cherubini, E. Eleftheriou, and S. Olcer, “Filtered multitone modulation for very high-speed digital subscriber lines," *IEEE J. Select. Areas Commun.*, vol. 20, no. 5, June 2002, pp. 1016-1028.

[30] N. Zhao, F. Pu, X. Xu, and N. Chen, “Cognitive wideband spectrum sensing using cosine-modulated filter banks," *Int. J. Electron.*, vol. 102, no. 11, 2015, pp. 1890-1901.

[31] P. Siohan, C. Siclet, and N. Lacaille, “Analysis and design of OFDM-OQAM systems based on filterbank theory," *IEEE Trans. Signal Process.*, vol. 50, no. 5, May 2002, pp. 1170–1183.

[32] V. Vakilian, T. Wild, F. Schaich, S. ten Brink, and J.-F. Frigon, “Universal-filtered multi-carrier technique for wireless systems beyond LTE," in *Proc. IEEE GLOBECOM Broadband Wireless Access Workshop*, Dec. 2013, pp. 223-228.

[33] T. Wild, F. Schaich, and Y. Chen, “5G air interface design based on universal filtered (UF-) OFDM," in *Int. Conf. Dig. Sig. Proc. (DSP)*, 2014, pp. 699–704.

[34] F. Schaich and T. Wild, “Waveform contenders for 5G - OFDM vs. FBMC vs. UFMC", *Proc. of 6th Int. Symp. on Commun., Control, and Signal Process.*, Athens, Greece, May 2014, pp.457-460.

[35] X. Wang, T. Wild, F. Schaich, A. Fonseca dos Santos, “Universal Filtered Multi-Carrier with Leakage-Based Filter Optimization", in *Proc. of European wireless Conference*, 2014, May 2014.

[36] X. Wang, T. Wild, F. Schaich and S. ten Brink, “Pilot-Aided Channel Estimation for Universal Filtered Multi-Carrier," in *Vehicular Technology Conf. (VTC Fall)*, Boston, MA, 2015.

[37] F. Schaich and T. Wild, “Relaxed Synchronization Support of Universal Filtered Multi-Carrier including Autonomous Timing Advance," in *IEEE Int. Symp. on Wireless Commun. Syst. (ISWCS)*, Barcelona, Aug. 2014.

[38] X. Wang, “Channel Estimation and Equalization for 5G Wireless Communication Systems," Master’s thesis, University of Stuttgart, 2014.

[39] E. Axell et al., “Spectrum Sensing for Cognitive Radio: State-of-the-Art and Recent Advances," *IEEE Journal on Selected Areas in Commun.*, vol. 29, no. 3, Mar. 2012, pp. 101–16.

[40] H. Kobayashi, B. L. Mark, W. Turin, *Probability, Random Processes, and Statistical Analysis*, Cambridge Univ. Press, 2012.

[41] A. Winkelbauer, “Moments and absolute moments of the normal distribution." [Online]. Available: `http://arxiv.org/pdf/1209.4340.pdf`

[42] A. Goldsmith, *Wireless Communications*, Cambridge Univ. Press, 2005.

[43] A. Svensson, “An overview of adaptive modulation schemes for known and predicted channels," in *Proc. of the IEEE*, vol. 95, no. 12, Dec. 2007, pp. 2322-2336.

[44] A. Antoniou, *Digital Signal Processing*, McGraw-Hill, 2006.

[45] J.O. Smith, *Spectral Audio Signal Processing*, W3K Publishing, 2011.

[46] P. Lynch, “The Dolph–Chebyshev Window: A Simple Optimal Filter", *Monthly Weather Review*, Vol. 125, Apr. 1997, pp.655-660.

[47] C.L. Dolph, “A current distribution for broadside arrays which optimizes the relationship between beam width and side lobe level", in *Proc. IRE*, June 1946, pp. 335-348.

[48] (2017, August 3). *Chebyshev polynomials* [Online]. Available: `https://en.wikipedia.org/wiki/Chebyshev_polynomials`

[49] M. Nardon and P. Pianca, “Simulation techniques for generalized Gaussian densities," Dept. of Applied Mathematics, University of Venice, Working Paper no. 145/2006, Nov. 2009.

[50] A. Taherpour, M. Nasiri-Kenari, and S. Gazor, “Multiple antenna spectrum sensing in cognitive radios," in *IEEE Trans. Wireless Commun.*, vol.9, Feb. 2010, pp. 814–823.